scientific reports

Check for updates

OPEN

A novel hyperbolic tangent-augmented controller framework for temperature control in jacketed continuous stirred tank reactors

Davut Izci[1], Serdar Ekinci[2], İrfan Ökten[2], Rıdvan Fırat Çınar[3], Mostafa Rashdan[4], Mohammad Salman[4]✉, Burcu Bektaş Güneş[5] & Mohd Ashraf Ahmad[6]

Accurate temperature regulation of jacketed continuous stirred tank reactors (CSTRs) remains a challenging task due to strong nonlinearities, tight coupling between mass and energy balances, and sensitivity to disturbances and operating-point variations. In this study, a novel augmented proportional–integral–derivative (PID) controller incorporating a hyperbolic tangent nonlinearity (APID-T) is proposed for robust temperature control of an exothermic CSTR. The controller structure extends the classical PID framework by embedding a bounded nonlinear term that enhances transient shaping and robustness while preserving simplicity and practical implementability. The tuning of the APID-T parameters is formulated as a constrained nonlinear optimization problem, where a composite objective function combining normalized overshoot and integral squared error is minimized. To solve this problem efficiently, the recently developed Schrödinger optimizer (SRA) is employed, exploiting its balanced exploration–exploitation mechanism. A detailed nonlinear dynamic model of the jacketed CSTR is considered, and stability characteristics around the nominal operating point are examined to ensure meaningful closed-loop operation. The proposed SRA-based APID-T design is extensively evaluated through comparative simulations against several state-of-the-art metaheuristic optimizers and alternative controller structures, including PI, PID with filter, two-degree-of-freedom PID, and fractional-order PID controllers. Performance is assessed using statistical indicators, convergence behavior, and time-domain response metrics under identical optimization settings. In addition, widely used error performance criteria, including the integral squared error, integral time absolute error, and integral time squared error, are computed to provide a comprehensive quantitative assessment of the tracking performance. The results demonstrate that the SRA-tuned APID-T controller consistently achieves lower objective-function values, faster convergence, reduced settling time, and significantly smaller overshoot compared with the competing approaches. Furthermore, frequency-domain analysis based on the Bode characteristics of the linearized open-loop system confirms favorable stability margins, supporting the robustness of the proposed control structure. Additional stability and robustness evaluations are conducted under practical non-ideal conditions, including feed-temperature disturbances, measurement noise, and multiple setpoint variations, where the controller maintains stable and accurate temperature regulation across the considered operating scenarios.

Keywords Augmented PID with tanh term (APID-T), Temperature regulation, Schrödinger optimizer, Robustness, Metaheuristics

Jacketed continuous stirred tank reactors (CSTRs) are widely employed in chemical and biochemical industries due to their flexibility, high productivity, and suitability for continuous operation[1]. However, accurate temperature regulation in such reactors remains a persistent and challenging control problem. This difficulty

[1]Department of Electrical and Electronic Engineering, Bursa Uludag University, 16059 Bursa, Turkey. [2]Department of Computer Engineering, Bitlis Eren University, 13100 Bitlis, Turkey. [3]Department of Computer Engineering, Batman University, 72100 Batman, Turkey. [4]College of Engineering and Technology, American University of the Middle East, Egaila 54200, Kuwait. [5]Department of Computer Engineering, Istanbul Gedik University, İstanbul, Turkey. [6]Faculty of Electrical and Electronics Engineering Technology, Universiti Malaysia Pahang Al-Sultan Abdullah, Pahang, Malaysia. ✉email: mohammad.salman@aum.edu.kw

primarily arises from the strongly nonlinear nature of the underlying reaction kinetics, the tight coupling between mass and energy balances, and the exponential dependence of reaction rates on temperature[2,3]. In exothermic CSTRs, these characteristics may lead to multiple steady states, pronounced transient sensitivity, and potential thermal runaway if the temperature is not properly regulated. Consequently, the design of effective and reliable temperature control strategies for CSTRs continues to attract considerable research attention[4–6].

Classical proportional–integral–derivative (PID) controllers are still dominant in industrial practice owing to their simple structure, ease of implementation, and intuitive tuning[7,8]. Nevertheless, for nonlinear processes such as jacketed CSTRs, conventional PID controllers often exhibit limited performance when operating conditions deviate from the nominal point[9]. Large setpoint changes, external disturbances, and measurement noise can significantly degrade transient response, resulting in excessive overshoot, long settling times, or even instability. To overcome these limitations, numerous enhanced control strategies have been reported in the literature, including sliding mode control schemes[10], intelligent algorithms-tuned PID controllers[11], two-degree-of-freedom (2-DOF) PID controllers[12], fractional-order PID (FOPID) controllers[9], model reference adaptive controllers[13], and various nonlinear or intelligent control approaches[14–20]. While these methods can improve performance, they often increase structural complexity, require additional tuning parameters, or suffer from practical implementation challenges.

Recent studies have also investigated advanced dual-loop and hybrid control strategies specifically designed for unstable or integrating CSTR dynamics. For instance, Kumar and Raja proposed a unified fractional indirect internal model control (IMC)-based hybrid dual-loop strategy capable of stabilizing unstable and integrating CSTR processes while achieving improved disturbance rejection and setpoint tracking performance[21]. Similarly, Kumari et al. introduced a hybrid dual-loop control method for dead-time second-order unstable inverse-response plants and demonstrated its effectiveness through a CSTR case study[22]. More recently, Das et al.[23] presented a dual-loop PID control strategy aimed at improving ramp tracking performance and disturbance rejection in unstable CSTR systems. These approaches highlight the growing interest in multi-loop and hybrid control architectures for handling complex reactor dynamics and improving regulation performance in challenging operating conditions. Recent research has also explored fractional-order and nonlinear control frameworks to improve the regulation performance of CSTR systems. For example, Mukherjee et al.[24] proposed an improved fractional augmented control strategy that enhances disturbance rejection and transient performance in nonlinear reactor dynamics. In another study, an optimal fractional-order IMC-based[25] cascade control approach with a dead-time compensator was introduced to stabilize unstable process dynamics and improve closed-loop robustness[26]. Furthermore, fractional-order adaptive and nonlinear control methodologies have been investigated for CSTR systems, including Lyapunov-based model reference adaptive control schemes[27] and standalone fractional backstepping controllers[28]. These approaches demonstrate the growing interest in fractional-order and nonlinear control paradigms for handling the strong nonlinearities and instability characteristics inherent to chemical reactor systems. Nevertheless, many of these strategies introduce additional structural complexity and require multiple fractional parameters, which may complicate practical implementation and tuning.

Another important trend in recent CSTR control studies is the use of metaheuristic optimization algorithms for controller tuning[29]. By formulating controller design as an optimization problem, metaheuristics enable systematic tuning of controller parameters with respect to well-defined performance criteria[30]. A wide range of algorithms inspired by natural, physical, or social phenomena has been successfully applied to CSTR temperature control[31–34]. Despite these advances, two key gaps can be identified in the existing literature. First, most studies focus on optimizing the parameters of linear controller structures, while the intrinsic nonlinearity of the process is handled indirectly through tuning rather than being explicitly addressed in the controller structure itself. Second, although many metaheuristic algorithms have been applied, comparative evidence demonstrating consistent performance improvements under identical conditions remains limited, particularly when robustness against disturbances, noise, and varying setpoints is considered simultaneously.

Motivated by these observations, this study proposes a novel augmented PID controller incorporating a hyperbolic tangent nonlinearity[35–37], referred to as the APID-T controller. The proposed structure preserves the simplicity and interpretability of the classical PID framework while embedding a smooth and bounded nonlinear component that enhances adaptability to large errors and operating-point variations. The hyperbolic tangent term provides a saturation-like behavior that strengthens control action near the operating point and limits excessive actuation during large transients, thereby improving robustness and transient shaping without introducing discontinuities or excessive complexity. To systematically determine the controller parameters, the tuning problem is formulated as a constrained nonlinear optimization task, in which both transient overshoot and cumulative tracking error are simultaneously minimized.

For solving this optimization problem, the recently developed Schrödinger optimizer[38] is employed. This algorithm combines wave-based exploration and particle-based exploitation mechanisms, enabling an effective balance between global search and local refinement. Its suitability for complex, nonlinear optimization problems makes it a promising candidate for controller tuning in challenging process-control applications. In this work, the Schrödinger optimizer is used to tune the parameters of the proposed APID-T controller and its performance is rigorously assessed against several contemporary metaheuristic optimizers under identical conditions.

In light of the above presentation, the main contributions of this study can be summarized as (1) a novel hyperbolic tangent–augmented PID controller is introduced for temperature regulation of jacketed CSTRs, explicitly addressing process nonlinearity while maintaining a simple and implementable structure; (2) the controller tuning problem is formulated using a composite objective function that jointly penalizes normalized overshoot and integral squared error, ensuring balanced transient and steady-state performance; (3) the Schrödinger optimizer is systematically evaluated for this control application and its performance is benchmarked against multiple state-of-the-art metaheuristic algorithms using statistical indicators and convergence analyses;

(4) comprehensive simulation studies are conducted on a nonlinear CSTR model, including comparative evaluations with conventional proportional-integral (PI), PID with filter (PIDf), two-degree-of-freedom PID (2-DOF PID), and fractional-order PID (FOPID) controllers; (5) robustness and practical applicability are verified under non-ideal conditions involving feed-temperature disturbances, measurement noise, and multiple sequential setpoint changes.

The results demonstrate that the SRA-tuned APID-T controller achieves faster convergence during optimization, lower objective-function values, reduced settling time, and significantly smaller overshoot compared with both alternative optimizers and conventional controller structures. Moreover, stable and accurate temperature regulation is maintained under disturbances, noise, and varying operating conditions. These findings confirm that embedding a bounded nonlinear augmentation within the PID framework, combined with an effective metaheuristic tuning strategy, provides a powerful and practical solution for temperature control of nonlinear jacketed CSTRs.

Dynamic behavior of jacketed continuous stirred tank reactors

Jacketed continuous stirred tank reactors (CSTRs) constitute one of the most frequently studied reactor configurations in chemical process dynamics because of their strong coupling between mass and energy balances[9]. Their behavior becomes especially rich when the underlying reaction is exothermic, as the interaction between heat generation and heat removal may produce multiple steady-states, non-linear transients, and, in certain parameter regimes, instabilities[39]. A schematic representation of the system studied in this work is displayed in Fig. 1, where a perfectly mixed reactor is equipped with an external cooling jacket whose temperature is adjusted to regulate the internal energy balance.

In the configuration considered here, a single irreversible, first-order exothermic reaction $A \rightarrow B$ proceeds in a well-mixed liquid phase[40]. Feed enters the reactor at a prescribed volumetric flow rate and temperature, while the exit stream leaves at the same composition and temperature as the bulk fluid, owing to the perfect-mixing assumption. Heat generated by reaction is continuously removed through the reactor walls into a cooling jacket whose inlet temperature serves as a manipulated variable. This arrangement is typical of many industrial reactors, including polymerization and specialty chemical processes, where temperature control is essential to maintain selectivity, prevent thermal runaway, and ensure safe operation.

The modeling framework adopted in this study follows the classical formulation based on constant density, constant volume, constant physical properties, and perfect mixing in both the reactor and the jacket[40]. The baseline parameter set used for dynamic simulations, drawn from standard CSTR literature, is summarized in Table 1. These values include the feed concentration C_{Af}, feed temperature T_f, reactor volume V, density ρ,

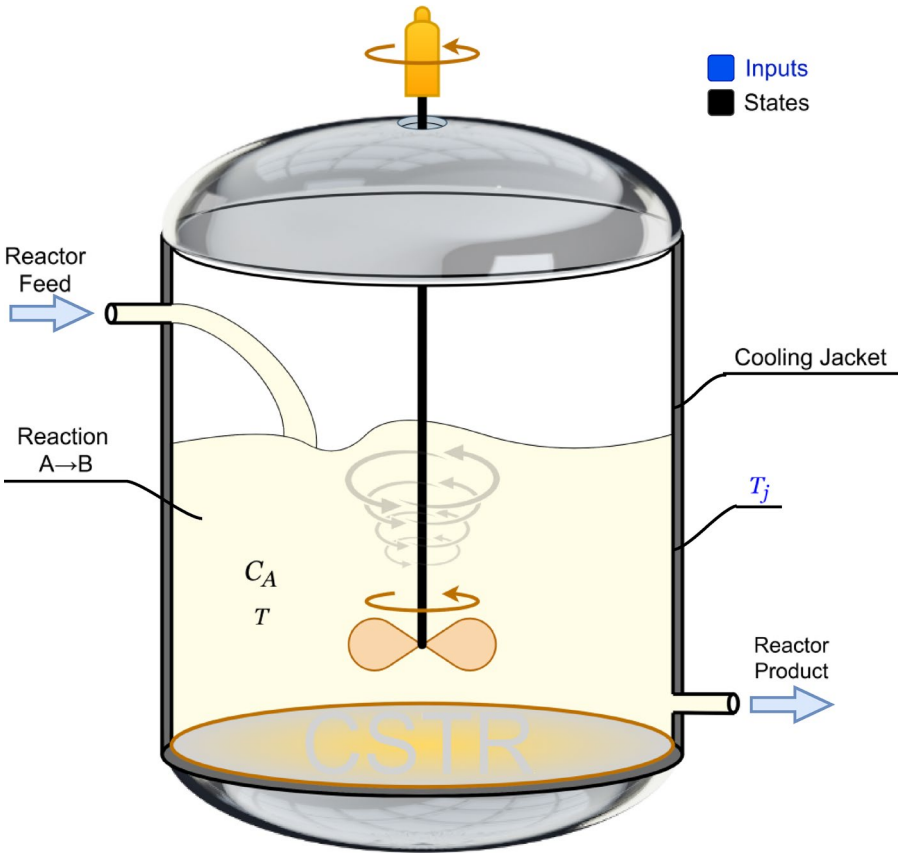

Fig. 1. Continuous stirred tank reactor with cooling jacket.

Variable	Value
T_f (Feed temperature)	350 K
$-\Delta H$ (Heat of reaction)	50,000 J/mol
UA (Overall heat-transfer coefficient × area)	50,000 J/min K
k_0 (Pre-exponential factor)	72×10^9 min^{-1}
ρ (Density)	1000 g/L
E/R (Activation energy over gas constant)	8750 K
C_{Af} (Feed concentration)	1 mol/L
c_p (Heat capacity)	0.239 J/g K
F (Feed flow rate)	100 L/min
V (Reactor volume)	100 L

Table 1. Baseline parameters for the CSTR model[41].

heat capacity c_p, heat-transfer coefficient–area product UA, kinetic parameters k_0 and E/R, T_j is cooling jacket temperature, C_A is the concentration of reactance A, T is the reactance temperature and the heat of reaction $-\Delta H$. The normal operating point corresponding to these values (used as the nominal steady-state for analysis) is $T_j = 300$ K, $T = 324.4754$ K, $C_A = 0.877253$ mol/L.

Two coupled nonlinear differential equations describe the evolution of the concentration of reactant A and the reactor temperature. The material balance on component A can be written as:

$$V\frac{dC_A}{dt} = F(C_{Af} - C_A) - Vr \tag{1}$$

where the reaction rate per unit volume is given by the Arrhenius expression[40].

$$r = k_0 e^{\left(-\frac{E}{RT}\right)} C_A \tag{2}$$

The energy balance accounts for enthalpy carried by the flowing streams, heat released by reaction, and heat removed through the jacket.

$$V\rho\, c_p \frac{dT}{dt} = F\rho\, c_p(T_f - T) + (-\Delta H)Vr - UA(T - T_j) \tag{3}$$

Equations (1)–(3) describe a two-state nonlinear dynamical system whose state vector is $x = [C_A, T]^T$. When written in standard state-variable form, the system becomes as follows.

$$\frac{dC_A}{dt} = \frac{F}{V}(C_{Af} - C_A) - r \tag{4}$$

$$\frac{dT}{dt} = \frac{F}{V}(T_f - T) + \frac{(-\Delta H)}{\rho\, c_p} r - \frac{UA}{V\rho\, c_p}(T - T_j) \tag{5}$$

These equations are identical in structure to the well-established diabatic CSTR model and capture the essential interplay between reaction kinetics, flow dilution, and heat removal.

The steady-state operating points of the reactor are obtained by imposing $dC_A/dt = 0$ and $d\mathrm{T}/dt = 0$. Substituting Eqs. (4) and (5) into the latter form yields the algebraic pair given below.

$$\frac{F}{V}(C_{Af} - C_A) - k_0 e^{\left(-\frac{E}{RT}\right)} C_A = 0 \tag{6}$$

$$\frac{F}{V}(T_f - T) + \frac{(-\Delta H)}{\rho\, c_p} k_0 e^{\left(-\frac{E}{RT}\right)} C_A - \frac{UA}{V\rho\, c_p}(T - T_j) = 0 \tag{7}$$

For many parameter combinations (including the values listed in Table 1), Eqs. (6) and (7) may admit multiple physically meaningful solutions. This classical multiplicity arises from the competition between heat generation (which accelerates with increasing temperature) and heat removal (which depends linearly on the reactor–jacket temperature difference). The nominal operating point supplied above corresponds to the intermediate root of this system for the selected parameters.

The dynamic response of the system depends strongly on its initial conditions and the chosen jacket temperature. When perturbed from steady-state, the reactor may relax to a low-temperature/high-concentration branch, a high-temperature/low-concentration branch, or remain near the intermediate point which is subjected to the stability characteristics of each solution. Simulations conducted using Eqs. (4) and (5) reveal several important qualitative features consistent with classical CSTR behavior:

1. Depending on the initial temperature and concentration, trajectories may converge to one of several steady-states.
2. For exothermic reactions under insufficient cooling, the intermediate solution typically acts as a saddle point. Small disturbances grow, directing the reactor either toward a lower-temperature state (where reaction is weak) or toward a high-temperature state (where reaction dominates).
3. Because the Arrhenius term varies exponentially with temperature, even modest deviations in T substantially alter the reaction rate, causing the temperature to accelerate upward or decay downward depending on the competing heat-removal term.

The dynamic trends observed here mirror the behavior described in the foundational CSTR literature, where the interplay of strong nonlinearity and heat-release mechanisms gives rise to ignition/extinction features, hysteresis, and sometimes oscillatory regimes for other sets of parameters.

To characterize the stability of a steady-state ($C_{A,s},\ T_s$), the governing equations may be linearized about this point. Let $x = \begin{bmatrix} C_A - C_{A,s} \\ T - T_s \end{bmatrix}$ and $u = [\ T_j - T_{j,s}\ ]$; the linearized form is $\dot{x} = Ax + Bu$. The Jacobian matrix A contains the partial derivatives of Eqs. (4) and (5) with respect to C_A and T. Using the standard notation from the literature, the elements are:

$$A_{11} = -\frac{F}{V} - k_s, A_{12} = -C_{A,s}k'_s \tag{8}$$

$$A_{21} = \frac{(-\Delta\ H)}{\rho\ c_p}k_s, A_{22} = -\frac{F}{V} - \frac{UA}{V\rho\ c_p} + \frac{(-\Delta\ H)}{\rho\ c_p}C_{A,s}k'_s \tag{9}$$

where $k_s = k_0 e^{\left(-\frac{E}{RT_s}\right)}$ and $k'_s = k_s\left(\frac{E}{RT_s^2}\right)$. The eigenvalues of A determine the local stability. Negative real parts imply a stable steady-state and positive real parts indicate an unstable one. For the baseline parameters in Table 1, the eigenvalues computed at the nominal operating point are both negative, confirming that the steady-state at $T = 324.4754$ K and $C_A = 0.877253$ mol/L is locally stable under the specified jacket temperature.

Schrödinger optimizer

The Schrödinger optimizer (SRA)[38] employs a dual-phase mechanism that governs the search process by dynamically alternating between wave-based exploration and particle-based exploitation. The entire operational flow is built upon the process whose flow-chart is given in Fig. 2, and the mathematical structure is defined by following formulation. These structure links concepts from quantum wave mechanics with Newtonian deterministic motion, yielding an adaptive framework capable of globally exploring the search space while refining solutions locally as the iterations progress.

Initially, all search agents are generated through random sampling within the defined lower and upper bounds of the search space. This initialization step is expressed as:

$$x_i = lb + rand \cdot\ (ub - lb) \tag{10}$$

for lb for lower bound and ub for upper bound. This formulation provides a uniform distribution of the initial population and prevents premature clustering around narrow regions of the domain. Such diversity is essential since the subsequent wave-based updates depend on ψ -values evaluated at different spatial locations. A suitably distributed population yield meaningful ψ -differences, which later drive broad exploration across the search space. After initialization, the objective function for each candidate solution is computed, and the current best and worst positions are identified. These positions serve as anchors for both exploration and exploitation updates.

The exploration phase relies on probabilistic updates derived from the wave function. The core element of this phase is the wave function defined as:

$$\psi\ (x_i, t) = \sin\left(x_i\right) \tag{11}$$

where x_i denotes the current spatial position of the search agent within the decision space, and t represents the iteration index interpreted as the discrete time parameter governing the evolution of the wave function. Simplified form above, originates from the infinite potential well model and provides a computationally effective alternative to the full Schrödinger equation. Although simplified, this function keeps the essential oscillatory characteristics needed to create constructive and destructive interference patterns through the search space. These interference patterns guide exploration by amplifying ψ -differences between regions, therefore directing candidate solutions toward more informative areas. The wave-based exploration mechanism is implemented using (12) and (13):

$$x_{i+1} = x_{best} + [\text{rand} * z_c * (\ h * (\psi\ (\ x_{\text{best}}, t) - \psi\ (x_{\text{worst}}, t\ )) + p\,[i] * (\psi\ (\ x_{\text{rand1}}, t) - \psi\ (x_i, t) + \psi\ (x_{\text{rand2}}, t\ ))\ )] / \psi\ (x_i, t) \tag{12}$$

$$x_{i+1} = x_i + [\text{rand} * z_c * (\ h * (\psi\ (\ x_{\text{best}}, t) - \psi\ (x_{\text{worst}}, t\ )) + p\,[i] * (\psi\ (\ x_{\text{rand1}}, t) - \psi\ (x_i, t) + \psi\ (x_{\text{rand2}}, t\ ))\ )] / \psi\ (x_i, t) \tag{13}$$

where the value of the function $\psi\ (x_{best},\ t)$ is evaluated at the best position, while $\psi\ (x_{worst},\ t)$ corresponds to the worst position. The terms $\psi\ (x_{rand1},\ t)$ and $\psi\ (x_{rand2},\ t)$ denote the values of the function at randomly selected positions, and $\psi\ (x_i,\ t)$ is the value at the current position. The parameter z_c decreases linearly from one to zero. These equations generate new positions by combining global ψ -differences with local interactions

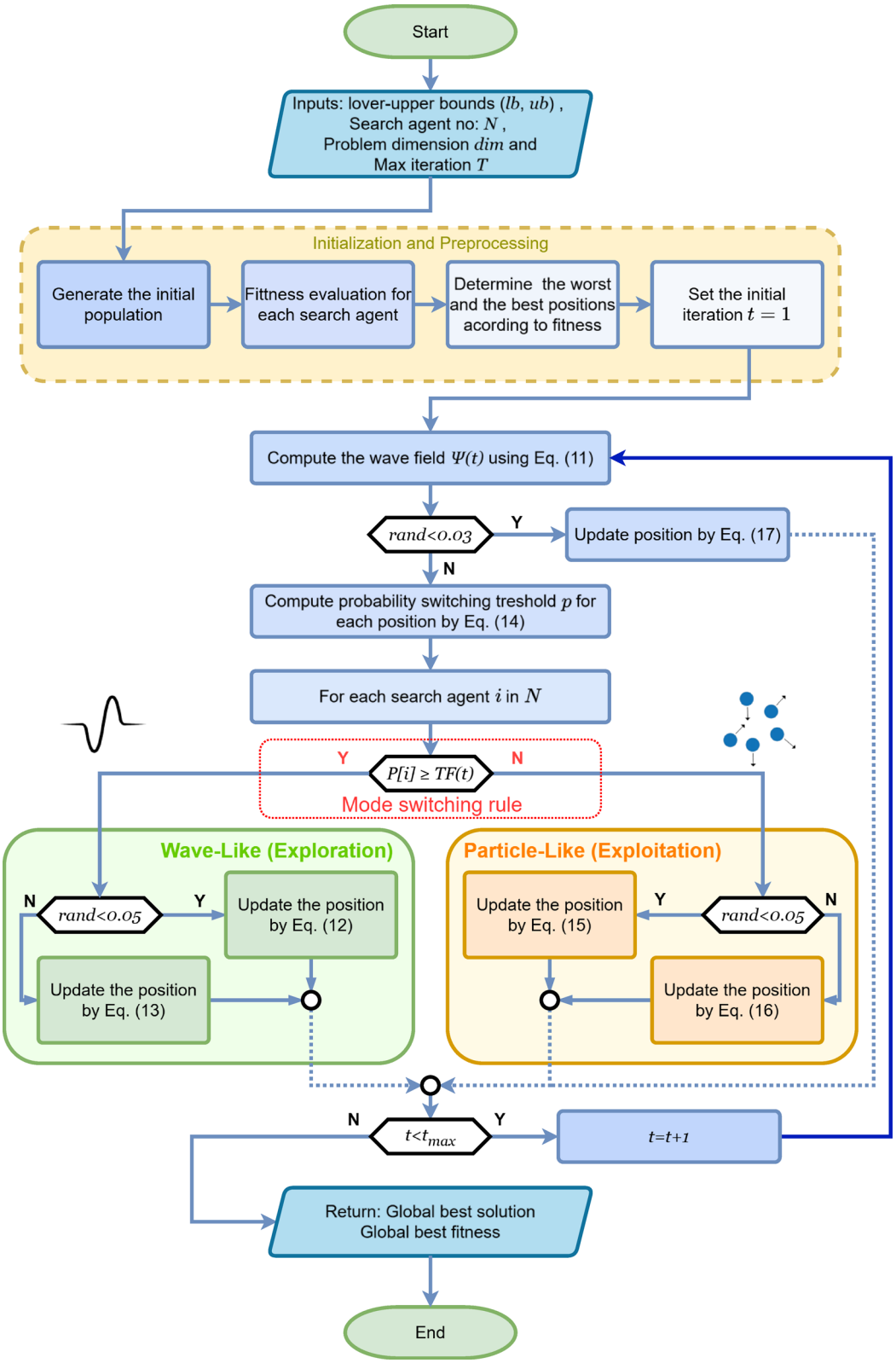

Fig. 2. Workflow for Schrödinger optimizer.

among randomly sampled agents. The term $\psi\left(x_{\text{best}}, t\right) - \psi\left(x_{\text{worst}}, t\right)$ leverages the contrast between the most promising and least promising regions, encouraging directed progression toward better areas. Additionally, the term involving random agents introduces stochasticity and maintains diversity. The normalization by $\psi\left(x_i, t\right)$ stabilizes updates and prevents extreme jumps.

The parameter $p[i]$, computed via Eq. (14):

$$p[i] = \left(\frac{N-i}{N}\right)^2 \quad , \tag{14}$$

acts as an adaptive weighting factor that decreases with the agent index, allowing earlier agents in the population experience stronger wave-like behaviour. Here i is the agent index defined as $i = 0,1,\ldots,N-1$, ensuring that $p[0] = 1$ and the weighting term decreases monotonically toward the last agent. When used alongside the time-varying transition function $TF(t)$, this parameter shapes how quickly each agent shifts from exploration to exploitation. Thus, $p[i]$ integrates population structure directly into the transition mechanism.

The exploitation phase is based on a deterministic update inspired by Newtonian motion. The primary update rule is given in Eqs. (15),

$$x_{i+1} = k \cdot \ rand + 2x_i - x_{i-1} \quad . \tag{15}$$

This update incorporates a second-order difference term $2x_i - x_{i-1}$, which models momentum and promotes steady movement within promising regions. The random factor $k \cdot rand$ injects controlled variability, preventing stagnation along deterministic trajectories. To intensify local search and strengthen convergence around high-quality regions, an alternative exploitation step is introduced in Eqs. (16),

$$x_{i+1} = x_{\text{best}} - rand \cdot \ u\left(x_{\text{rand1}} - x_{\text{rand2}}\right) \quad . \tag{16}$$

This update pulls the search trajectory toward the current global best solution while incorporating local perturbations derived from randomly selected agents. The combination effectively tightens the search around optimal areas while preserving the flexibility needed to escape shallow local minima.

To further protect against stagnation, a low-probability restart mechanism is included. Equation (17) specifies that when a random draw satisfies $rand < 0.03$:

$$x_{i+1} = rand \cdot \ (ub - lb) + lb \text{ if } rand < 0.03 \tag{17}$$

the agent's position is reinitialized. This 3% probability preserves diversity and prevents the optimizer from collapsing prematurely into narrow basins of attraction. Because the event is rare, it does not disrupt the overall progression but effectively breaks stagnation when necessary.

The transition between exploration and exploitation is controlled by the adaptive threshold function $TF(t)$, defined in Eq. (18).

$$TF(t) = \left(\frac{t}{t_{max}}\right)^3 \tag{18}$$

This cubic form yields a slow increase during early iterations, promoting extended exploration, while accelerating the shift toward exploitation as t approaches $t_{\max}$. The comparison between $p[i]$ and $TF(t)$ determines the behavioral mode of each agent at each iteration, enabling a synchronized but flexible transition across the population.

Reaching the end of each iteration, the updated positions are evaluated, ψ-values are recalculated, and the global best solution is updated accordingly. The loop continues until the maximum iteration limit is reached, after which the best solution and its associated fitness are returned. Through this combination of probabilistic wave dynamics and deterministic particle motion, the Schrödinger optimizer achieves a balanced progression from global exploration to precise local refinement.

Proposed control structure

This section presents the proposed control framework developed for robust temperature regulation of the nonlinear jacketed CSTR system. First, the structural design and operational principles of the proposed controller are introduced and analyzed. The controller architecture is described in detail, highlighting how the classical proportional–integral–derivative (PID) actions are complemented by a bounded nonlinear augmentation to enhance robustness and transient performance under strong nonlinearities. Subsequently, the formulation of the nonlinear optimization problem used for controller tuning is provided. This includes the definition of the composite objective function, the imposed performance criteria, and the admissible bounds of the controller parameters. The relevant subsections establish a coherent control and optimization framework that forms the basis for the simulation studies and comparative performance evaluations presented in the subsequent section.

Novel augmented PID controller with a hyperbolic tangent component

In order to enhance regulation performance under strong nonlinearities and operating-point variations, a novel augmented PID controller incorporating a hyperbolic tangent term (APID-T) is proposed. The overall structure of the controller is illustrated in Fig. 3, where the conventional PID actions are complemented by a bounded nonlinear component designed to improve robustness and transient shaping without sacrificing simplicity. As depicted in Fig. 3, the control signal is generated from the tracking error e through four parallel paths. The proportional path scales the instantaneous error by the gain k_p, providing an immediate corrective action. The integral path, governed by the gain k_i, accumulates the error over time and is responsible for eliminating steady-state offsets. The derivative path introduces anticipatory action through the gain k_d, while a first-order

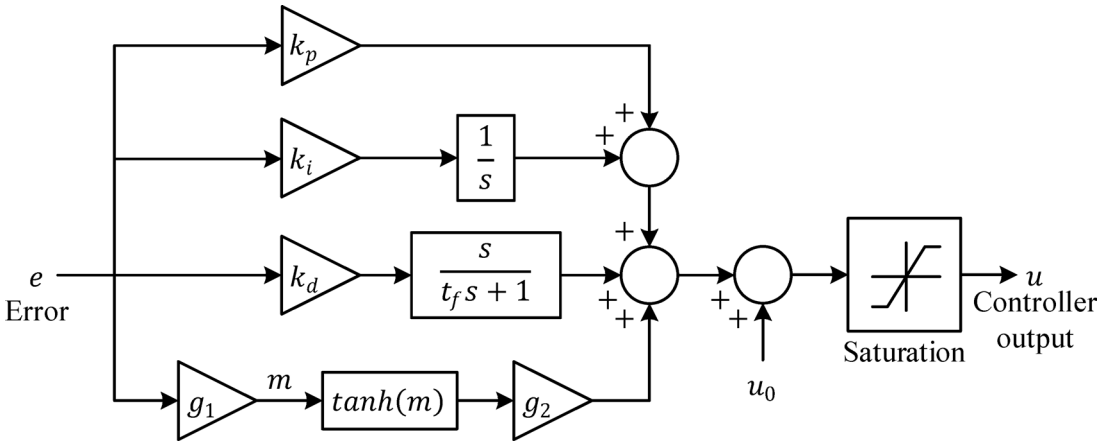

Fig. 3. Block diagram of APID-T controller.

filter with time constant t_f is employed to attenuate high-frequency noise amplification commonly associated with ideal differentiation. This filtered derivative term preserves the stabilizing effect of derivative action while maintaining implementability in practical systems.

Beyond the classical PID components, an additional nonlinear augmentation is introduced through a hyperbolic tangent[42] function. As shown in Fig. 3, the error signal is first scaled by the gain g_1, producing an internal variable m. This variable is then processed by the $tanh$ function, and the resulting bounded output is further scaled by the gain g_2 before being summed with the conventional PID contributions. The hyperbolic tangent function is inherently smooth and saturating, yielding an output confined to the interval $(-1, 1)$. As a result, the augmented term provides a nonlinear corrective action that grows approximately linearly for small errors but gradually saturates for large deviations.

This structure introduces several advantageous properties. For small tracking errors, the hyperbolic tangent term behaves almost linearly, effectively acting as an adaptive gain that reinforces the classical PID action near the operating point. For larger errors, the saturation characteristic limits the magnitude of the nonlinear contribution, thereby preventing excessive control effort and reducing the risk of actuator saturation or aggressive transients. In this sense, the parameters g_1 and g_2 may be interpreted as shaping factors that regulate the sensitivity and strength of the nonlinear augmentation, respectively. Following the summation of the proportional, integral, derivative, and hyperbolic tangent components, the composite control signal is passed through an explicit saturation block, as indicated in Fig. 3. This element reflects practical actuator constraints and ensures that the applied control input remains within admissible bounds. The inclusion of saturation at the controller output is particularly important for nonlinear processes such as jacketed CSTRs, where excessive manipulation of the jacket temperature may lead to undesirable operating regimes or physical limitations. Overall, the APID-T controller preserves the intuitive and widely accepted structure of the PID controller while embedding an additional nonlinear degree of freedom through the hyperbolic tangent term. This augmentation enables improved handling of nonlinear dynamics, enhances robustness against disturbances and parameter uncertainties, and allows smoother transient responses compared with purely linear PID designs. The gains k_p, k_i, k_d, t_f, g_1, and g_2 collectively define the controller behavior and are treated as decision variables in the subsequent optimization framework, where their values are systematically tuned to achieve superior temperature regulation performance.

Objective functions and bounds of nonlinear optimization problem

The tuning of the proposed APID-T controller is formulated as a constrained nonlinear optimization problem, in which the controller parameters are adjusted to achieve fast and accurate temperature regulation while limiting excessive transient excursions. To this end, a composite objective function is defined to simultaneously penalize overshoot and cumulative tracking error, thereby balancing transient performance with overall regulation quality. The scalar objective function minimized during optimization is expressed as:

$$F_{obj} = \sigma \cdot OS_{norm} + (1 - \sigma) \int_0^{t_{sim}} e^2(t)\, dt \tag{19}$$

where $e(t) = r(t) - y(t)$ denotes the instantaneous tracking error between the reactor temperature and its reference, and t_{sim} represents the total simulation horizon. In this study, the simulation time is fixed at $t_{\mathrm{sim}} = 20$ min, which is sufficient to capture both transient and steady-state behaviors of the nonlinear CSTR dynamics. The first term in Eq. (19) accounts for overshoot, which is quantified using a normalized formulation to ensure comparability across different operating conditions. Specifically, the normalized reactor temperature response is defined as:

$$y_{norm}(t) = \frac{y(t) - y_{init}}{y_{final} - y_{init}} \tag{20}$$

where y_{init} and y_{final} denote the initial and final steady-state reactor temperatures, respectively. Based on this normalized response, the normalized overshoot is computed as $OS_{norm} = \max(y_{norm}(t) - 1) \times 100$ which captures the maximum deviation above the desired normalized steady-state value. This formulation ensures that overshoot is penalized in a scale-independent manner and remains consistent with the imposed reference change. The second term in Eq. (19) represents the integral of the squared error (ISE)[43], which penalizes sustained deviations from the setpoint and promotes smooth convergence. The weighting factor $\sigma \in [0,1]$ determines the relative importance of overshoot suppression versus cumulative error minimization. In the present study, σ is selected as 0.125, assigning a higher emphasis to long-term regulation accuracy while still discouraging excessive overshoot. This choice was found to provide a suitable compromise between fast settling and conservative transient behavior for the highly nonlinear CSTR process.

During optimization, the reactor temperature setpoint is intentionally perturbed to evaluate the controller's dynamic performance. Specifically, the reference temperature is increased from 324.4754 to 344.4754 K at $t = 1$ min, corresponding to a step change of 20 K. This excitation is sufficiently large to challenge the nonlinear dynamics of the reactor and to reveal differences in controller robustness, transient shaping, and disturbance rejection capabilities. The decision variables of the optimization problem consist of the six APID-T controller parameters, namely the proportional gain k_p, integral gain k_i, derivative gain k_d, derivative filter time constant t_f, and the hyperbolic tangent scaling gains g_1 and g_2. To ensure physically meaningful and implementable solutions, each parameter is constrained within predefined bounds of $0.1 \leq k_p \leq 2$, $0.05 \leq k_i \leq 1$, $0.1 \leq k_d \leq 2$, $0.02 \leq t_f \leq 0.25$, $0.2 \leq g_1 \leq 5$ and $0.2 \leq g_2 \leq 5$. These bounds are selected to cover a wide yet realistic range of controller behaviors, preventing overly aggressive gains that could destabilize the reactor or cause actuator saturation, while still allowing sufficient flexibility for the optimizer to explore high-performance solutions. In particular, the bounds on g_1 and g_2 regulate the sensitivity and magnitude of the nonlinear hyperbolic tangent augmentation, ensuring that its contribution remains smooth and bounded.

The complete optimization loop, including objective-function evaluation, parameter updating via the SRA, and closed-loop simulation of the nonlinear CSTR model, is illustrated in Fig. 4. As shown in the figure, candidate controller parameters generated by the optimizer are injected into the APID-T structure, the resulting jacket temperature signal is applied to the nonlinear CSTR process, and the reactor temperature response is fed back to compute the objective function. This closed-loop procedure is repeated iteratively until convergence criteria are satisfied, yielding an optimized APID-T controller tailored to the nonlinear thermal dynamics of the jacketed CSTR.

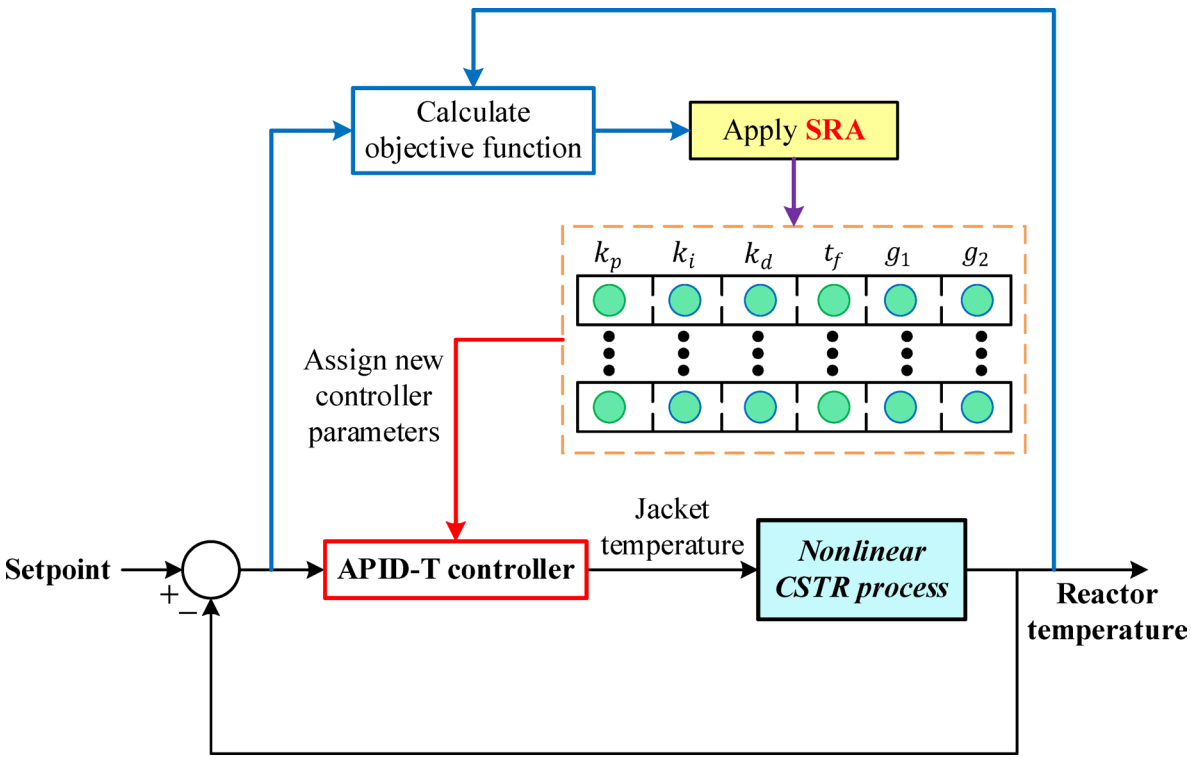

Fig. 4. The implementation of the proposed APID-T designed via SRA for CSTR process.

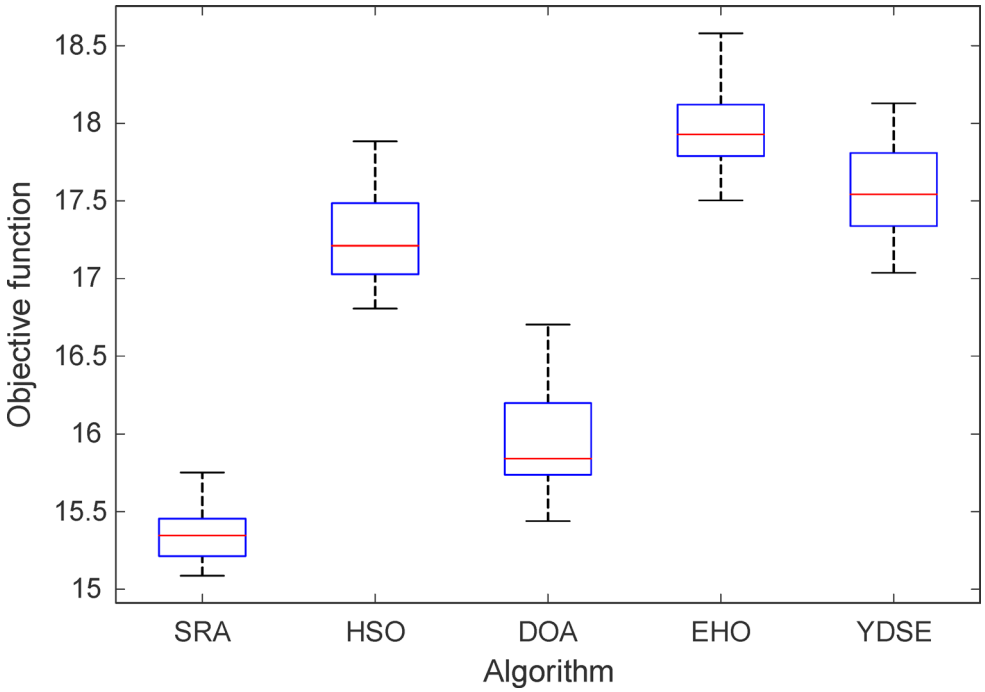

Fig. 5. Comparative boxplots obtained via SRA, HSO, DOA, EHO and YDSE for objective function values.

Index	SRA	HSO	DOA	EHO	YDSE
Minimum	15.0869	16.8064	15.4389	17.5033	17.0367
Maximum	15.7522	17.8837	16.7033	18.5798	18.1288
Average	15.3505	17.2438	15.9552	17.9579	17.5745
Standard Deviation	0.1887	0.2988	0.3211	0.2646	0.3037

Table 2. Numerical statistical results obtained via SRA, HSO, DOA, EHO and YDSE.

Simulation results and discussion

This section presents a comprehensive evaluation of the proposed control framework through systematic simulation studies. First, the effectiveness of the SRA is verified by benchmarking its optimization performance against several recent metaheuristic algorithms using statistical indicators, convergence characteristics, and objective-function distributions. Subsequently, the superiority of the proposed APID-T controller is examined through direct comparisons with conventional PI, PIDf, 2-DOF PID, and FOPID controllers under identical optimization settings, highlighting differences in transient response and tracking accuracy. Finally, the robustness and practical applicability of the proposed approach are assessed under non-ideal operating conditions, including external disturbances, measurement noise, and multiple sequential setpoint changes. Together, these analyses provide a detailed and coherent validation of both the optimization strategy and the proposed controller structure for nonlinear CSTR temperature regulation.

Performance verification of SRA

The performance of the proposed Schrödinger optimizer (SRA)[38] was systematically evaluated through a comparative study against four recently developed metaheuristic algorithms: holistic swarm optimization (HSO)[44], dream optimization algorithm (DOA)[45], elk herd optimizer (EHO)[46] and Young's double-slit experiment optimizer (YDSE)[47]. All algorithms were tested under identical conditions to ensure a fair and unbiased assessment. In each case, the APID-T controller parameters were optimized using a population size of 20, a maximum iteration count of 50, and 25 independent runs.

The statistical distribution of the objective-function values obtained from these repeated runs is illustrated in Fig. 5 through comparative boxplots. As observed, the SRA consistently yielded lower objective-function values compared with the competing algorithms. Moreover, the dispersion of results associated with SRA is noticeably narrower, indicating enhanced repeatability and robustness. In contrast, HSO, EHO, and YDSE exhibit wider interquartile ranges, reflecting higher sensitivity to initial population variations.

A quantitative summary of these observations is provided in Table 2. The SRA achieved the lowest minimum (15.0869) and average (15.3505) objective-function values among all tested methods, while also exhibiting the smallest standard deviation (0.1887). These results indicate that SRA not only converges toward

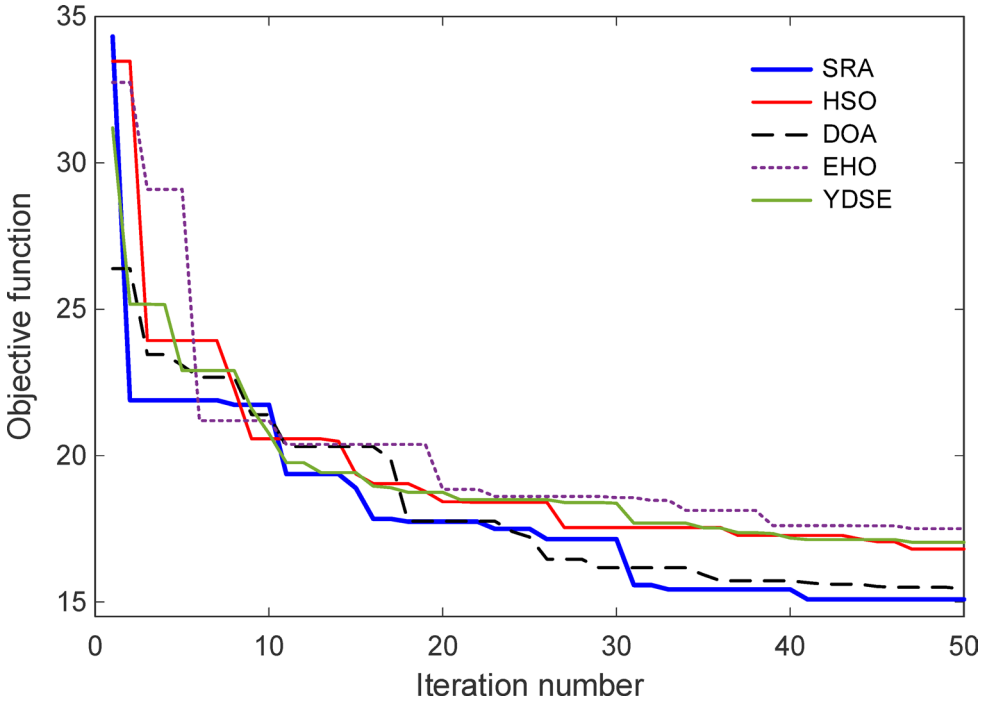

Fig. 6. Comparative convergence curves obtained via SRA, HSO, DOA, EHO and YDSE.

Parameter	SRA	HSO	DOA	EHO	YDSE
k_p	0.1718	0.2427	0.8219	0.4561	0.1893
k_i	0.4574	0.5323	0.5910	0.5490	0.6028
k_d	1.9920	1.6415	1.9976	1.8856	1.8783
t_f	0.2477	0.1727	0.1663	0.1442	0.1849
g_1	4.8919	4.9483	3.8385	4.7013	4.7682
g_2	4.2216	4.6084	4.4545	4.7920	3.2719

Table 3. Optimal APID-T parameters obtained via SRA, HSO, DOA, EHO and YDSE.

superior solutions but also maintains stable performance across multiple independent executions. Although DOA achieved a relatively competitive minimum value, its higher standard deviation suggests less consistent convergence behavior compared with SRA.

The convergence characteristics of all algorithms are further examined in Fig. 6, where the evolution of the objective function over iterations is presented. The SRA demonstrates a faster and smoother convergence trend, particularly during the early and mid-iteration stages. While other algorithms eventually approach lower objective-function regions, their convergence paths are generally slower and exhibit more pronounced oscillations. This behavior highlights the ability of SRA to effectively balance exploration and exploitation throughout the optimization process.

The optimized APID-T controller parameters obtained by each algorithm are listed in Table 3. Although all algorithms identify feasible parameter sets within the predefined bounds, the values obtained via SRA result in superior closed-loop performance, as confirmed by subsequent time-domain analyses. Notably, the SRA-tuned controller exhibits a well-balanced combination of proportional, integral, and derivative gains, alongside relatively high values of the nonlinear hyperbolic tangent gains g_1 and g_2, which contribute to improved transient shaping and robustness.

The closed-loop reactor temperature responses corresponding to each optimized controller are shown in Fig. 7, with a magnified view provided in Fig. 8. All controllers successfully track the imposed 20 K setpoint change; however, clear differences in transient behavior can be observed. The SRA-based APID-T controller reaches the desired temperature more rapidly and with visibly reduced overshoot compared with the alternatives.

These observations are quantitatively confirmed in Table 4, which reports key time-response metrics. The SRA-optimized controller achieves the shortest settling time (1.6248 min) and the lowest overshoot (0.0562 K), while also producing the smallest cumulative absolute error (2.7046). It is emphasized that the overshoot values reported in Table 4 are expressed in absolute temperature units (Kelvin) rather than percentages. Competing

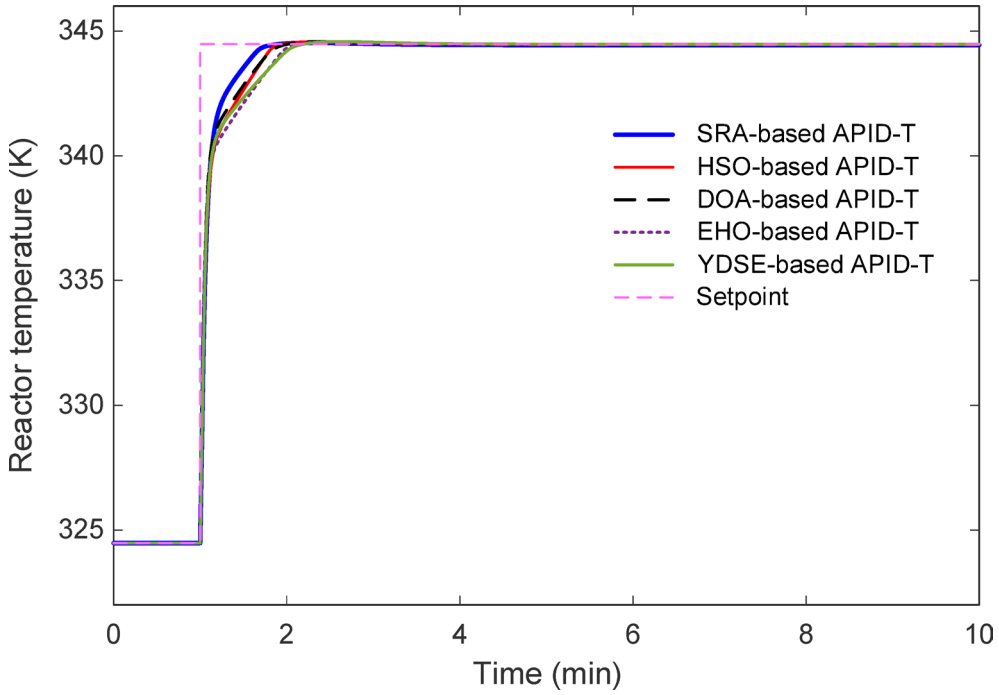

Fig. 7. Step response showing the reactor temperature change via SRA, HSO, DOA, EHO and YDSE.

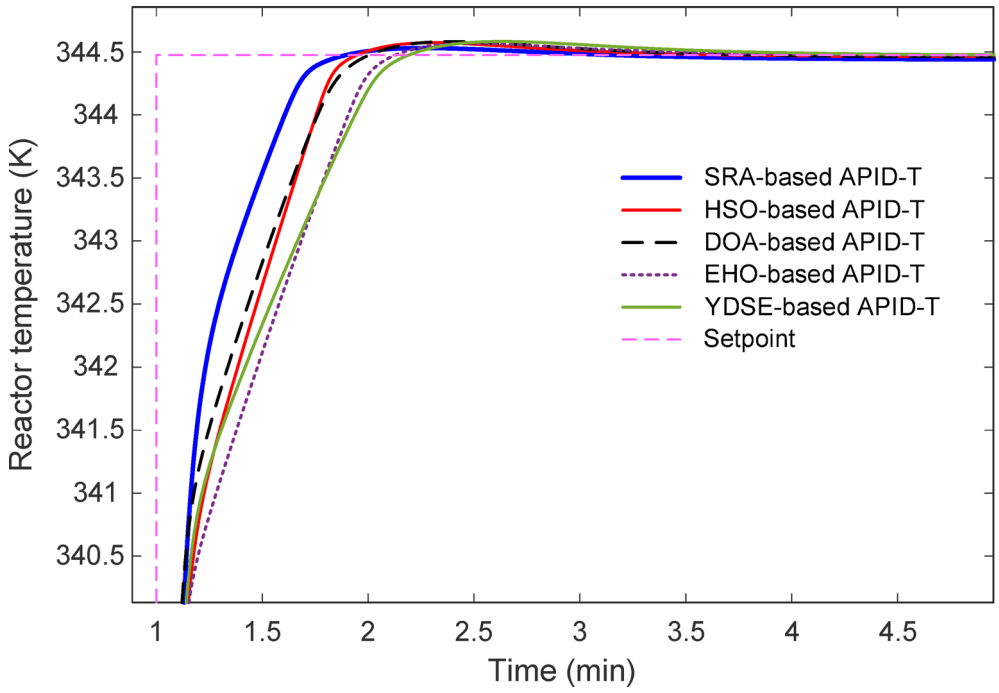

Fig. 8. Zoomed view of Fig. 7.

algorithms exhibit longer settling times and larger overshoot magnitudes, indicating comparatively less favorable transient responses.

Error performance metrics

To provide a more comprehensive quantitative evaluation of the control performance, several widely used error-based performance indices were computed based on the closed-loop simulation responses. In addition to the objective function employed during the optimization stage, three classical integral performance criteria were evaluated, namely the integral squared error (ISE), integral time absolute error (ITAE), and integral time

Time response metric	SRA	HSO	DOA	EHO	YDSE
Settling time (min)	1.6248	1.7696	1.7816	1.9241	1.9600
Peak (K)	344.5316	344.5736	344.5828	344.5691	344.5838
Overshoot (K)	0.0562	0.0981	0.1073	0.0937	0.1084
Cumulative absolute error	2.7046	2.9804	2.8203	3.2205	3.1132

Table 4. Comparative time response metrics.

Error metric	SRA	HSO	DOA	EHO	YDSE
ISE	17.2021	19.1372	17.5678	19.9369	19.3931
$ITAE$	8.3843	5.7476	5.6909	4.7280	4.1856
$ITSE$	18.3506	20.8342	18.9918	22.1956	21.4133

Table 5. Error performance metrics obtained for the APID-T controller tuned using different optimization algorithms.

squared error (ITSE). These indices characterize different aspects of the tracking error dynamics. The ISE metric is given in Eq. (21).

$$ISE = \int_0^{t_{sim}} e^2(t)\, dt \tag{21}$$

This metric penalizes large error magnitudes by squaring the instantaneous tracking error, thereby emphasizing transient deviations. The ITAE criterion is given in Eq. (22):

$$ITAE = \int_0^{t_{sim}} t\,|e(t)|\, dt \tag{22}$$

And it assigns increasing weight to errors occurring at later stages of the response, which promotes faster settling and improved steady-state behavior. Similarly, the ITSE index, given in Eq. (23), captures both the magnitude and duration of the error signal, providing an additional measure of persistent transient deviations.

$$ITSE = \int_0^{t_{sim}} te^2(t)\, dt \tag{23}$$

The computed values of these performance metrics for the considered optimization algorithms are summarized in Table 5, where the calculations were performed using the tracking error obtained from the closed-loop responses shown in Fig. 7. As can be observed, the SRA-based tuning approach achieves the lowest ISE value (17.2021) among the considered algorithms, indicating that it produces the smallest overall error energy throughout the simulation period. A similar trend is observed in the ITSE metric, where the SRA-based solution yields a value of 18.3506, which is again lower than the corresponding values obtained using HSO, DOA, EHO, and YDSE algorithms. This result suggests that the SRA-tuned APID-T controller effectively suppresses sustained transient errors during the regulation process. Although the ITAE value obtained with the SRA method (8.3843) is slightly higher than those obtained with some alternative optimization methods, the overall performance indicators collectively demonstrate that the SRA-based tuning framework provides a balanced trade-off between transient accuracy and error attenuation over the entire operating horizon. These quantitative metrics further confirm the effectiveness of the proposed optimization approach for tuning the APID-T controller in nonlinear CSTR temperature regulation.

Comparison with other controllers

To further assess the effectiveness of the proposed APID-T controller, a comparative study was conducted against several well-established control structures, namely the proportional–integral (PI)[48], PID with derivative filtering (PIDf)[49], two-degree-of-freedom PID (2-DOF PID)[12], and fractional-order PID (FOPID)[50] controllers. For the sake of fairness and consistency, all controllers were tuned using the same objective function, identical population size, and the same number of iterations, with the SRA employed as the tuning algorithm in every case. This setup ensures that the observed performance differences are attributable solely to the intrinsic control structures rather than to disparities in optimization conditions.

The mathematical formulations of the considered controllers, together with the optimal parameter values obtained via SRA, are summarized in Table 6. The PI controller represents the simplest structure, relying only

Controller type	Controller formula	Values of controller parameters tuned by SRA
PI	$u = \left(k_p + \frac{k_i}{s}\right) e$	$k_p = 3.2663,\ k_i = 0.2887$
PIDf	$u = \left(k_p + \frac{k_i}{s} + \frac{k_d s}{t_f s+1}\right) e$	$k_p = 1.1874,\ k_i = 0.6359,\ k_d = 0.7381,\ t_f = 0.2190$
2-DOF PID	$u = k_p\,[br - y] + \frac{k_i}{s} e + \frac{k_d s}{t_f s+1}\,[cr - y]$	$k_p = 1.3873,\ k_i = 0.9366,\ k_d = 1.4603,\ t_f = 0.6634,\ b = 0.9416,\ c = 0.8295$
FOPID	$u = \left(k_p + \frac{k_i}{s^\lambda} + k_d s^\mu\right) e$	$k_p = 1.9516,\ k_i = 0.2941,\ k_d = 1.4273,\ \lambda = 1.0313,\ \mu = 0.7298$

Table 6. The adopted controllers and their respective parameters tuned via SRA.

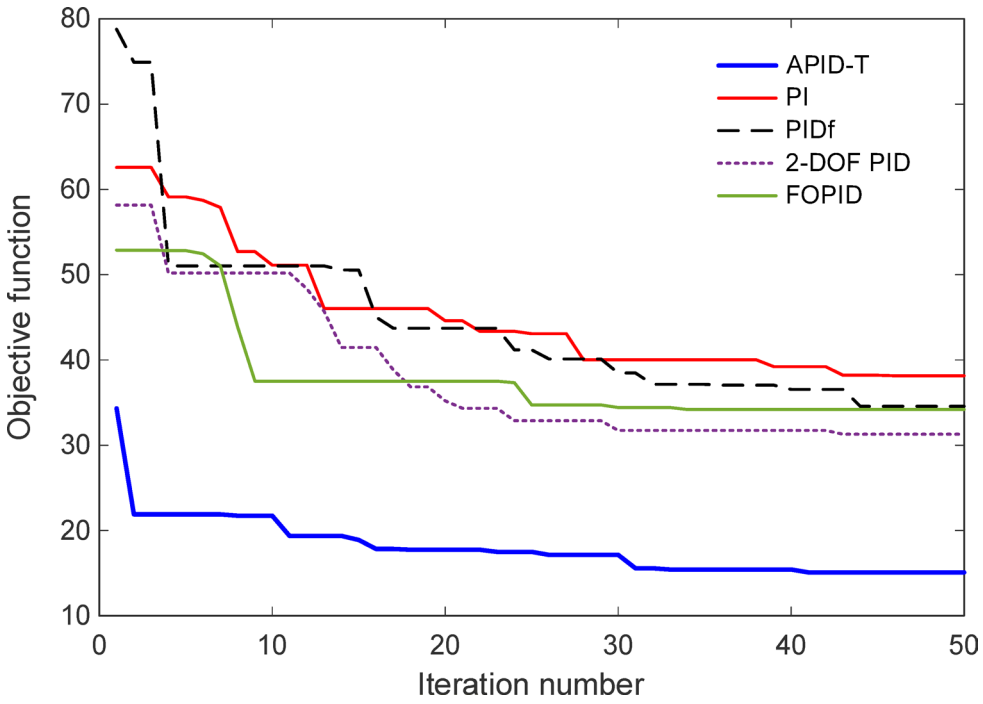

Fig. 9. Comparative convergence curves for different controller structures.

on proportional and integral actions. The PIDf controller extends this formulation by incorporating a derivative term equipped with a first-order filter to mitigate noise amplification. The 2-DOF PID introduces additional weighting factors on the reference signal, allowing partial decoupling between setpoint tracking and disturbance rejection. The FOPID controller generalizes the conventional PID structure by allowing non-integer orders of integration and differentiation, thereby increasing design flexibility at the expense of additional complexity. In contrast, the APID-T controller augments the classical PID framework with a bounded hyperbolic tangent term, providing nonlinear adaptability while retaining a relatively compact parameter set.

The convergence behavior associated with each controller structure is illustrated in Fig. 9. It can be observed that the optimization process associated with the APID-T controller converges more rapidly and toward a significantly lower objective-function value than those of the alternative controllers. The PI and PIDf structures exhibit slower convergence and stagnate at comparatively higher objective values, reflecting their limited ability to cope with the strong nonlinearities of the CSTR. The 2-DOF PID and FOPID controllers demonstrate improved convergence characteristics relative to PI and PIDf; however, their final objective-function values remain higher than that achieved by APID-T. This behavior highlights the advantage of embedding nonlinear compensation directly into the controller structure rather than relying solely on increased degrees of freedom or fractional dynamics.

The closed-loop reactor temperature responses for all controller types are depicted in Fig. 10. While all controllers are capable of tracking the imposed 20 K setpoint change, pronounced differences are evident in transient performance. The PI controller exhibits a large overshoot and a slow decay toward steady-state, indicative of insufficient damping. The PIDf controller reduces overshoot compared with PI but still suffers from sluggish settling. The 2-DOF PID and FOPID controllers provide more balanced responses, with reduced overshoot and faster convergence; nevertheless, their transients remain inferior to that of the APID-T controller, which reaches the target temperature smoothly and with minimal deviation.

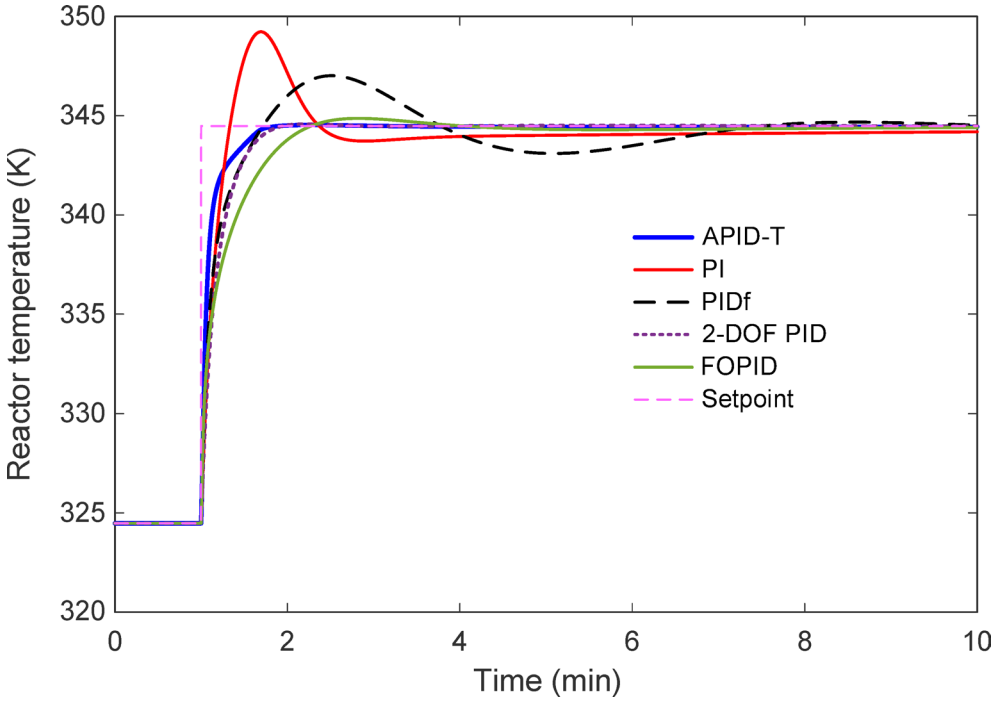

Fig. 10. Step response showing the reactor temperature change for different controller structures.

Time response metric	APID-T	PI	PIDf	2-DOF PID	FOPID
Settling time (min)	1.6248	6.5811	6.7929	1.7307	2.0935
Peak (K)	344.5316	349.2273	347.0152	344.5740	344.8653
Overshoot (K)	0.0562	4.7519	2.5398	0.0985	0.3899
Cumulative absolute error	2.7046	10.4243	9.9343	3.8728	6.2654

Table 7. Time response metrics obtained for different controller structures.

These qualitative observations are corroborated quantitatively by the time-domain performance indices reported in Table 7. The APID-T controller achieves the shortest settling time (1.6248 min), the lowest peak temperature, and the smallest overshoot magnitude (0.0562 K). In addition, it yields the minimum cumulative absolute error, confirming superior overall tracking accuracy. By contrast, the PI and PIDf controllers produce substantially larger overshoot values—expressed here in absolute temperature units (Kelvin)—and exhibit settling times exceeding 6 min. Although the 2-DOF PID and FOPID controllers markedly improve upon these results, they still fall short of the performance delivered by the APID-T structure. Overall, this comparative analysis demonstrates that the proposed APID-T controller provides a more favorable balance between fast transient response, minimal overshoot, and reduced cumulative error than the conventional PI, PIDf, 2-DOF PID, and FOPID controllers under identical optimization conditions. These results confirm that the incorporation of the hyperbolic tangent augmentation significantly enhances control effectiveness for the nonlinear CSTR system, thereby validating the superiority of the proposed approach.

Evaluation of control effectiveness under practical non-idealities

In this section, the robustness and practical applicability of the proposed SRA-optimized APID-T controller are examined under conditions that deviate from ideal assumptions. Specifically, two representative non-ideal scenarios are considered to reflect realistic industrial operation. Initially, the closed-loop performance is evaluated in the presence of external disturbances and sensor noise, where time-varying feed temperature changes and bounded measurement noise are simultaneously applied to assess disturbance rejection and noise tolerance. Subsequently, it investigates the tracking capability of the controller under multiple and sequential setpoint variations, aimed at verifying consistent performance across different operating levels. The following subsections provide a comprehensive assessment of the proposed control strategy's robustness, adaptability, and reliability under practical operating conditions. Although the simulations in this study were conducted using a widely adopted two-state nonlinear jacketed CSTR model, the proposed control framework is not restricted to this particular reactor representation. The APID-T controller operates solely on the tracking error and does not rely on a specific internal model structure, which makes it readily applicable to CSTR systems of different dynamic orders and configurations. In more detailed reactor models, additional states may arise

from multiple reaction pathways, concentration dynamics of intermediate species, catalyst deactivation effects, or extended heat-transfer mechanisms. Since the APID-T controller preserves the classical PID architecture while augmenting it with a bounded nonlinear term, its implementation remains independent of the number of process states. Therefore, the same controller structure and optimization framework can be directly applied to higher-order CSTR models, reactors with multiple reactions, or alternative thermal configurations such as multi-jacket or coil-based heat exchange systems. Only the tuning process would need to be repeated to account for the modified process dynamics. This property highlights the practical flexibility of the proposed approach and supports its potential applicability to a wide range of nonlinear chemical reactor systems encountered in industrial practice.

Evaluation of the system for disturbance and sensor noise

In order to assess the robustness of the proposed SRA-based APID-T controller under practical non-ideal operating conditions, its performance was further evaluated in the presence of external disturbances and measurement noise. Such conditions are unavoidable in real industrial implementations of jacketed CSTRs, where feed property variations and sensor imperfections may significantly influence closed-loop behavior. In this study, sensor noise was introduced as an additive measurement disturbance acting on the reactor temperature signal. The noise amplitude was bounded within the interval $[-0.1, 0.1]$ K, representing realistic thermal sensor fluctuations commonly encountered in industrial temperature measurements. The resulting noise profile, illustrated in Fig. 11, exhibits high-frequency variations superimposed on the measured signal, thereby challenging the controller's ability to maintain smooth and accurate regulation.

In addition to measurement noise, a structured external disturbance was applied through variations in the feed temperature T_f, which constitutes a dominant disturbance channel in CSTR dynamics. The disturbance profile was defined as a piecewise-constant signal, given in Eq. (24), where the feed temperature was sequentially shifted across multiple operating levels over a total simulation horizon of 100 min. Specifically, T_f was increased from its nominal value to a higher temperature, subsequently reduced below nominal, and finally restored to its original level. This disturbance pattern emulates realistic scenarios such as upstream process fluctuations or feed preheating inconsistencies. The complete disturbance and noise signals employed for this robustness test are depicted in Fig. 11.

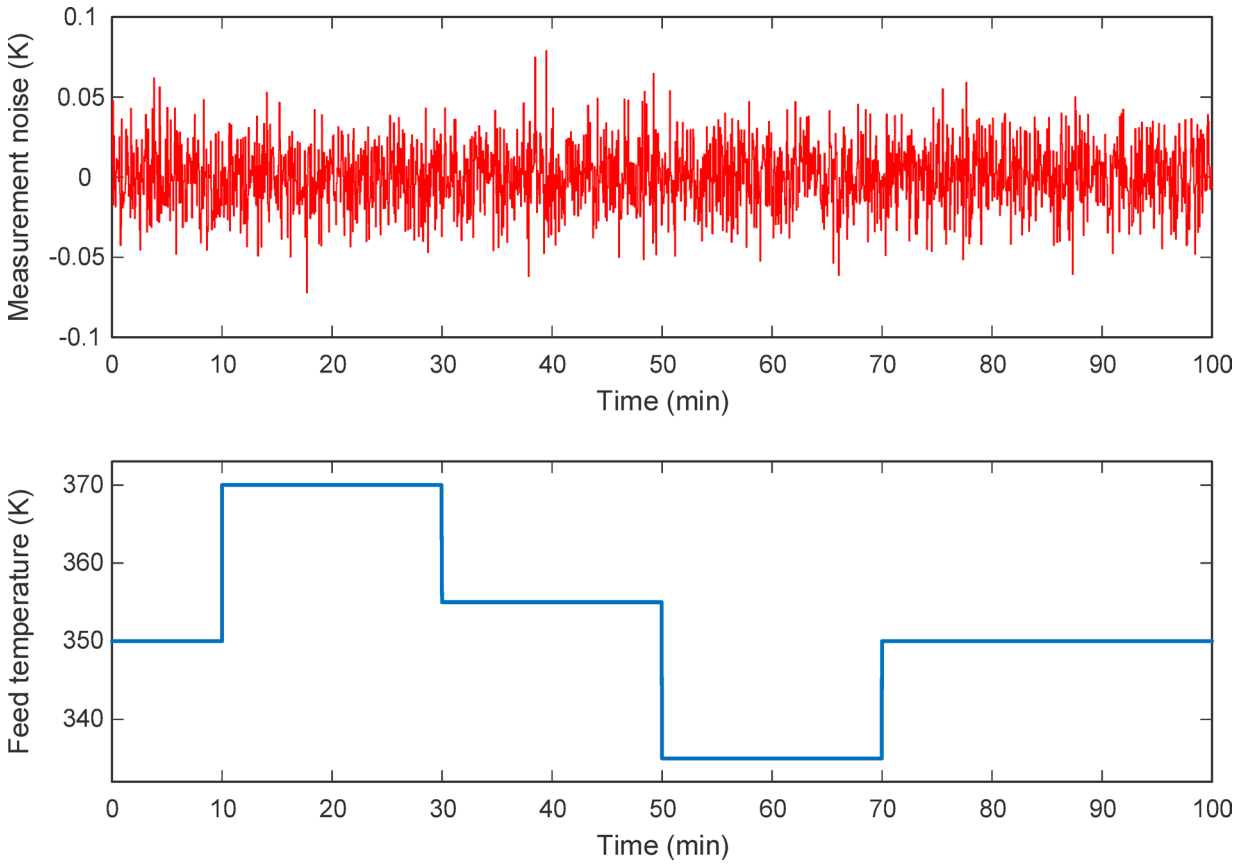

Fig. 11. The adopted external disturbance and noise signals for performance evaluation under practical non-idealities.

$$T_f = \begin{cases} 350\,K; & if\ \ 0 \leq\ t < 10\,min \\ 370\,K; & if\ \ 10 \leq\ t < 30\,min \\ 355\,K; & if\ \ 30 \leq\ t < 50\,min \\ 335\,K; & if\ \ 50 \leq\ t < 70\,min \\ 350; & if\ \ 70 \leq\ t < 100\,min \end{cases} \tag{24}$$

The closed-loop reactor temperature response obtained under these non-ideal conditions is presented in Fig. 12. Despite the simultaneous presence of bounded measurement noise and significant feed-temperature disturbances, the APID-T controller successfully preserved stable operation and accurate setpoint tracking. Following each abrupt change in T_f, transient deviations in reactor temperature were observed; however, these deviations remained limited in magnitude and were rapidly attenuated. The controller effectively rejected the disturbances and restored the reactor temperature to the desired setpoint without inducing oscillatory or unstable behavior. It is also noteworthy that the high-frequency measurement noise did not propagate into excessive control action. This behavior can be attributed to two key structural features of the proposed controller: the filtered derivative term, which mitigates noise amplification, and the bounded hyperbolic tangent augmentation, which limits nonlinear corrective action under large or rapidly varying errors. As a result, the control signal remained smooth, and no chattering or aggressive actuation was observed throughout the simulation. Overall, the results demonstrate that the SRA-tuned APID-T controller exhibits strong robustness against both external disturbances and sensor noise. The ability to maintain satisfactory temperature regulation under such adverse conditions confirms the practical suitability of the proposed control strategy for nonlinear CSTR applications, where uncertainty, disturbances, and measurement imperfections are inherent.

Performance evaluation for different setpoints

In addition to disturbance and noise rejection, the capability of the proposed SRA-based APID-T controller to handle frequent reference variations was investigated through a multi–setpoint tracking experiment. Such scenarios are representative of practical CSTR operation, where temperature setpoints may be adjusted repeatedly to accommodate changes in production requirements, operating modes, or safety constraints. The reference trajectory applied to the reactor temperature is defined by the piecewise-constant profile given in Eq. (25), which introduces successive step changes of varying magnitudes and directions over a total simulation horizon of 50 min. This sequence includes both upward and downward transitions around the nominal operating point, thereby providing a stringent test of the controller's adaptability and robustness.

$$T = \begin{cases} 324.4754\,K; & if\ \ 0 \leq t < 1\,min \\ 349.4754\,K; & if\ \ 1 \leq t < 10\,min \\ 329.4754\,K; & if\ \ 10 \leq t < 20\,min \\ 339.4754\,K; & if\ \ 20 \leq t < 30\,min \\ 344.4754\,K; & if\ \ 30 \leq t < 40\,min \\ 324.4754\,K; & if\ \ 40 \leq t < 50\,min \end{cases} \tag{25}$$

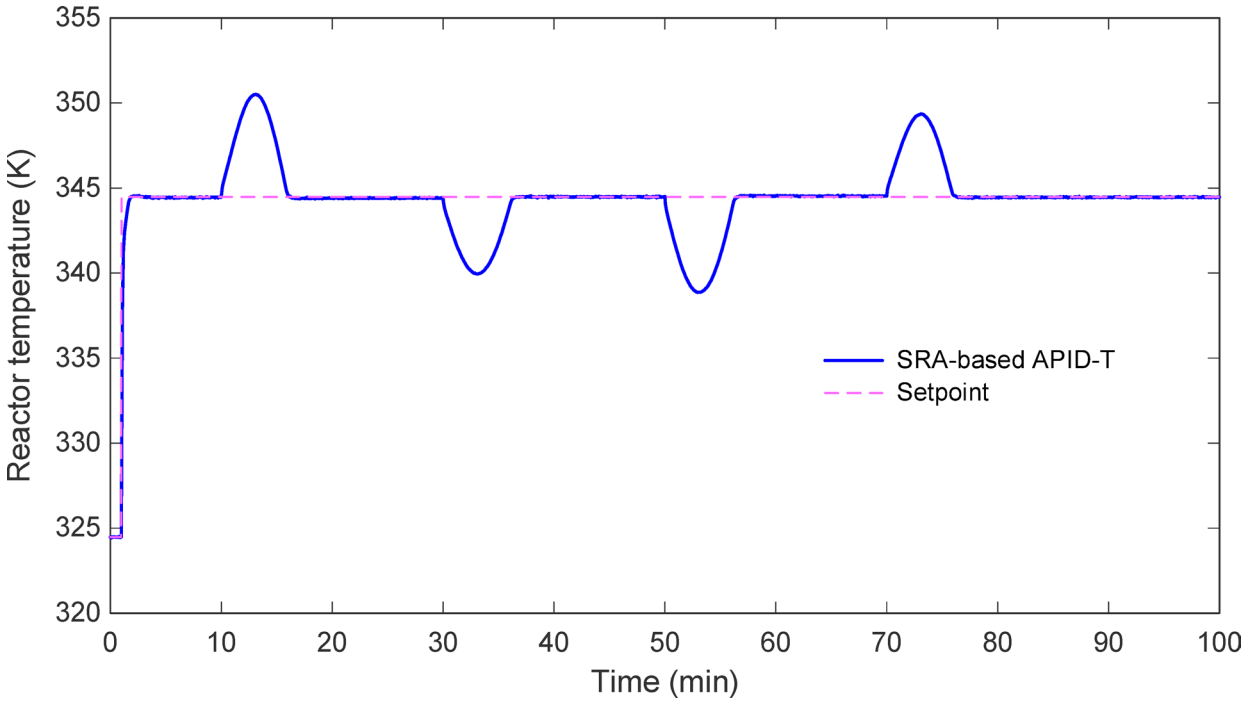

Fig. 12. Step response showing the reactor temperature change with respect to non-ideal conditions.

As specified in Eq. (25), the reactor temperature reference is initially maintained at the nominal steady-state value of 324.4754 K and is subsequently shifted to higher and lower levels at predefined time intervals. These setpoint changes span a wide operating range, including increases up to 349.4754 K and decreases down to 329.4754 K, before finally returning to the nominal value. The adopted profile is intentionally nonuniform, ensuring that the controller response is evaluated under asymmetric and nonrepetitive transitions rather than simple periodic steps.

The closed-loop reactor temperature response corresponding to this reference sequence is illustrated in Fig. 13. It can be observed that the APID-T controller successfully tracks each setpoint change with high accuracy and stable behavior. Following every reference transition, the reactor temperature converges rapidly to the new desired level without inducing sustained oscillations or excessive overshoot. Both upward and downward setpoint changes are accommodated smoothly, indicating that the controller maintains consistent performance across different operating regions of the nonlinear CSTR dynamics. Particularly noteworthy is the controller's ability to manage downward setpoint changes, which are often more challenging in exothermic reactors due to residual heat generation and thermal inertia. As shown in Fig. 13, the APID-T controller effectively suppresses prolonged decay tails and prevents undershoot during these transitions. This behavior can be attributed to the combined action of the filtered derivative term and the bounded hyperbolic tangent augmentation, which together provide anticipatory damping while limiting aggressive corrective action. Consequently, the control signal remains well behaved, and the reactor temperature follows the reference trajectory in a controlled and predictable manner. Overall, the results obtained from this multi–setpoint tracking test demonstrate that the proposed APID-T controller exhibits strong adaptability to varying operating requirements. The ability to accurately track successive and nonuniform setpoint changes, while preserving fast convergence and smooth transients, confirms the suitability of the proposed control strategy for practical CSTR applications where operating conditions are rarely fixed. These findings further reinforce the effectiveness of the SRA-tuned APID-T controller in delivering robust and reliable temperature regulation over a wide range of operating scenarios.

Frequency response analysis

In addition to the time-domain simulations presented earlier, the frequency-domain characteristics of the controlled system were also examined to assess the robustness and stability properties of the proposed control framework. For this purpose, the Bode diagram of the linearized open-loop system corresponding to the SRA-tuned APID-T controller was evaluated. The resulting frequency-response characteristics are illustrated in Fig. 14, where the magnitude and phase responses are plotted over a wide frequency range. These plots provide valuable insights into the gain behavior and phase dynamics of the controlled system and allow important stability indicators to be extracted. From the obtained Bode diagram, the phase margin was determined to be approximately 92°, indicating a substantial stability buffer against model uncertainties and unmodeled dynamics. Such a large phase margin suggests that the closed-loop system can tolerate moderate variations in system parameters without compromising stability. In addition, the delay margin was estimated to be 0.0266 min, demonstrating that the controller maintains stable operation even in the presence of small time-delay effects that may arise from measurement, computation, or actuator dynamics in practical implementations. The analysis also

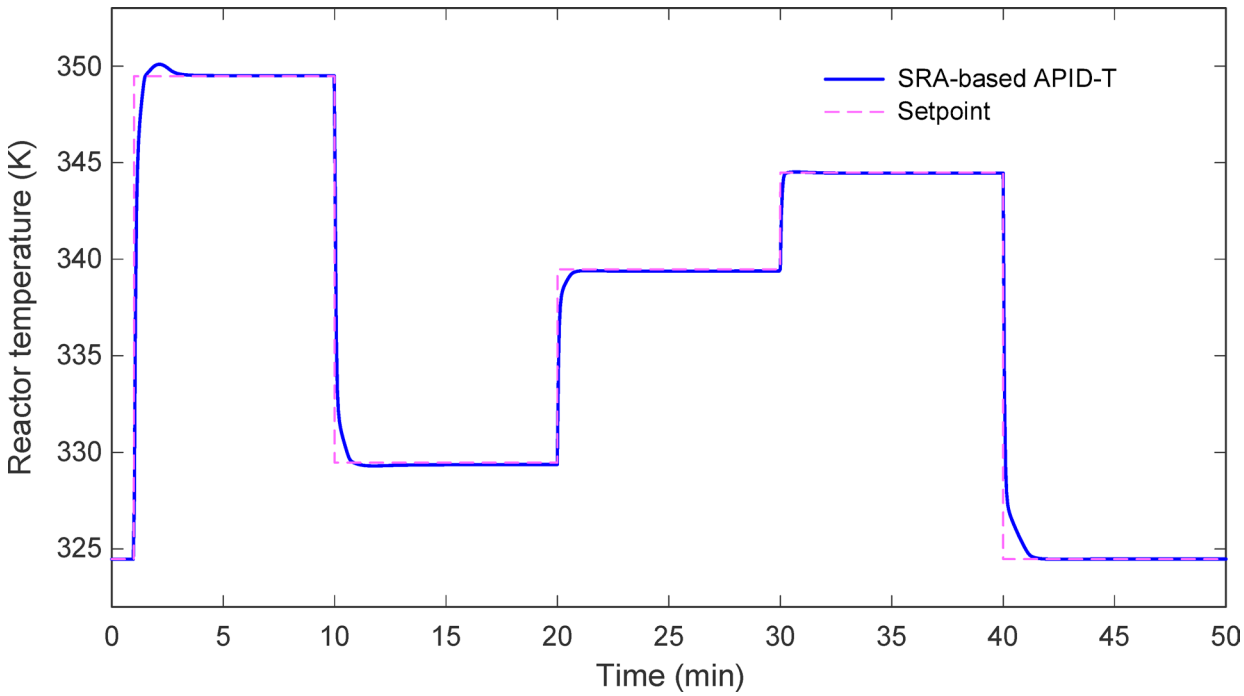

Fig. 13. Performance of the proposed method for different setpoints defined in Eq. (25)

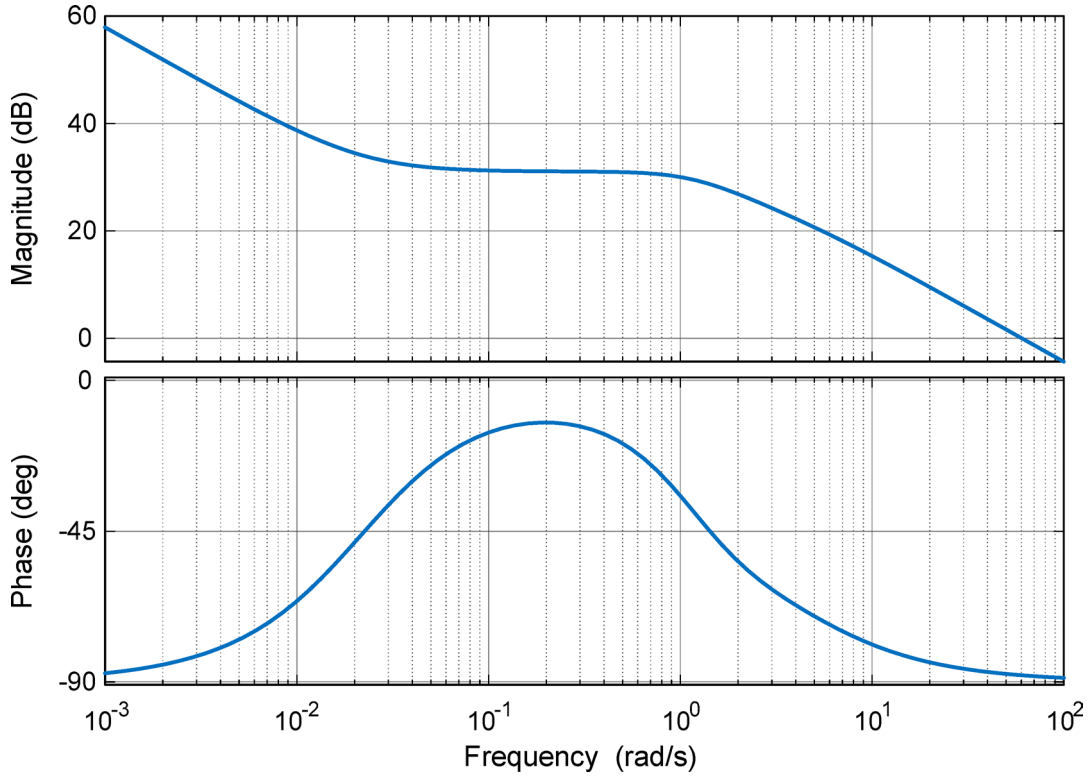

Fig. 14. Bode plot of open-loop SRA-based APID-T controlled system.

reveals a peak gain value of approximately 398 dB, which characterizes the maximum gain magnitude within the considered frequency range. Overall, the frequency-response analysis confirms that the proposed SRA-based APID-T controller provides not only favorable transient performance in the time domain but also robust stability characteristics in the frequency domain. The relatively large phase margin and acceptable delay margin indicate that the proposed control framework possesses sufficient robustness for practical implementation in nonlinear CSTR temperature regulation problems.

Conclusion

In this study, a novel controller, named APID-T, has been developed for robust temperature regulation of a nonlinear jacketed continuous stirred tank reactor. The proposed control structure preserves the simplicity and intuitive appeal of the classical PID framework while introducing a bounded nonlinear augmentation that enhances adaptability and robustness under strong process nonlinearities and operating-point variations. The hyperbolic tangent component was shown to provide smooth, saturation-like behavior, reinforcing control action near the operating point and preventing excessive actuation during large transients. A detailed nonlinear dynamic model of the exothermic CSTR was adopted, and its steady-state and stability characteristics were analyzed to establish a meaningful control baseline. The tuning of the APID-T parameters was formulated as a constrained nonlinear optimization problem, where a composite objective function combining normalized overshoot and integral squared error was minimized. The recently proposed Schrödinger optimizer was employed as the tuning mechanism, exploiting its balanced exploration–exploitation capability to efficiently search the controller parameter space.

Extensive simulation studies demonstrated that the SRA-tuned APID-T controller consistently outperformed several state-of-the-art metaheuristic optimizers in terms of convergence speed, solution quality, and statistical robustness. Furthermore, comparative evaluations against conventional PI, PIDf, 2-DOF PID, and FOPID controllers confirmed the superiority of the proposed structure. The APID-T controller achieved faster settling times, significantly reduced overshoot, and lower cumulative tracking errors under identical optimization conditions, highlighting the benefit of embedding nonlinear compensation directly into the controller design. The quantitative simulation results further highlight the effectiveness of the proposed approach. The SRA-optimized APID-T controller achieved a settling time of 1.6248 min, an overshoot magnitude of only 0.0562 K, and a cumulative absolute error of 2.7046, outperforming all benchmark controllers considered in this study. In comparison, the conventional PI and PIDf controllers produced significantly slower responses, with settling times exceeding 6 min and overshoot values reaching 4.7519 K and 2.5398 K, respectively. Even advanced structures such as the 2-DOF PID and FOPID controllers exhibited higher overshoot levels (0.0985 K and 0.3899 K) and larger cumulative tracking errors (3.8728 and 6.2654) than the proposed method. From the optimization perspective, the Schrödinger optimizer also demonstrated superior search capability, achieving the lowest objective-function statistics among the tested algorithms with a minimum value of 15.0869, an average

value of 15.3505, and a standard deviation of 0.1887 across 25 independent runs. In addition to the objective-function evaluation, complementary error-based performance metrics, including the ISE, ITAE, and ITSE, were also analyzed to provide a broader quantitative assessment of the closed-loop tracking performance. Further insights into the stability characteristics of the proposed control scheme were obtained through frequency-domain analysis. The Bode diagram of the linearized open-loop system corresponding to the SRA-tuned APID-T controller revealed a phase margin of approximately 92° and a delay margin of 0.0266 min, indicating a comfortable stability reserve and strong tolerance to moderate model uncertainties and delay effects. These findings, together with the well-damped closed-loop responses observed in the time domain, confirm that the proposed controller ensures stable operation of the nonlinear CSTR system across the investigated operating conditions. The robustness and practical applicability of the proposed approach were further validated under non-ideal operating conditions. The controller maintained stable and accurate temperature regulation in the presence of bounded measurement noise and structured feed-temperature disturbances. In addition, reliable performance was observed under multiple and sequential setpoint changes, demonstrating strong adaptability across a wide operating range. These results indicate that the proposed APID-T controller is well suited for realistic CSTR applications, where disturbances, noise, and varying production requirements are unavoidable.

Data availability

All related data are presented within the manuscript.

Received: 1 January 2026; Accepted: 3 April 2026
Published online: 08 April 2026

References

1. Cui, X., Mannan, M. S. & Wilhite, B. A. Towards efficient and inherently safer continuous reactor alternatives to batch-wise processing of fine chemicals: CSTR nonlinear dynamics analysis of alkylpyridines N-oxidation. *Chem. Eng. Sci.* **137**, 487–503. https://doi.org/10.1016/j.ces.2015.06.012 (2015).
2. Liu, Y. C. et al. A comparative study of continuous operation between a dynamic baffle crystallizer and a stirred tank crystallizer. *Chem. Eng. J.* **367**, 278–294. https://doi.org/10.1016/j.cej.2019.02.129 (2019).
3. Skupin, P., Laszczyk, P. & Metzger, M. Bifurcation analysis of a hybrid continuous stirred tank reactor with imperfect mixing in the cooling jacket. *IFAC-PapersOnLine* **52**, 334–339. https://doi.org/10.1016/j.ifacol.2019.11.802 (2019).
4. Siddiqui, M. A., Anwar, M. N. & Laskar, S. H. Control of nonlinear jacketed continuous stirred tank reactor using different control structures. *J. Process Control* **108**, 112–124. https://doi.org/10.1016/j.jprocont.2021.11.005 (2021).
5. Jencia, J., Vijay Anand, L. D., Hepsiba, D. Analysis of different control strategies in continuous stirred tank reactor. In *2022 6th International Conference on Devices, Circuits and Systems (ICDCS)* 407–412. (IEEE, 2022). https://doi.org/10.1109/ICDCS54290.2022.9780726
6. Hussein, S. A., El-Affendi, M. & El-Latif, A. A. Advanced control strategies for nonlinear continuous stirred tank reactors using emerging technologies 292–307 (2025). https://doi.org/10.1007/978-3-031-91235-1_26
7. Mohindru, P. Review on PID, fuzzy and hybrid fuzzy PID controllers for controlling non-linear dynamic behaviour of chemical plants. *Artif. Intell. Rev.* **57**, 97. https://doi.org/10.1007/s10462-024-10743-0 (2024).
8. Shamsuzzoha, M. & Lloyds Raja, G. (eds) *PID Control for Linear and Nonlinear Industrial Processes* (IntechOpen, 2023). https://doi.org/10.5772/intechopen.100749.
9. Izci, D. et al. Neighborhood centroid opposition-based flood algorithm for optimizing fractional-order PID control in nonlinear heat exchanger dynamics. *Chaos Solitons Fractals* **204**, 117729. https://doi.org/10.1016/j.chaos.2025.117729 (2026).
10. Wallam, F. & Memon, A. Y. A robust control scheme for nonlinear non-isothermal uncertain jacketed continuous stirred tank reactor. *J. Process Control* **51**, 55–67. https://doi.org/10.1016/j.jprocont.2016.11.001 (2017).
11. Khanduja, N. & Bhushan, B. Intelligent control of CSTR using IMC-PID and PSO-PID controller. In *2016 IEEE 1st International Conference on Power Electronics, Intelligent Control and Energy Systems (ICPEICES)* 1–6. (IEEE, 2016). https://doi.org/10.1109/ICPEICES.2016.7853329
12. Ekinci, S., Izci, D., Jabari, M. & Ma'arif, A. Enhanced temperature control of continuous stirred tank reactors using QIO-based 2-DoF PID controller. *J. Robot. Control* **6**, 1340–1346. https://doi.org/10.18196/jrc.v6i3.26586 (2025).
13. Kiran, M. G. & Pati, U. C. Comparative analysis of performance of different controllers for a continuous stirred tank reactor. In *2019 IEEE International Conference on Innovations in Communication, Computing and Instrumentation (ICCI)* 117–122. (IEEE, 2019). https://doi.org/10.1109/ICCI46240.2019.9404457
14. Gupta, P., Kumar, V., Rana, K. P. S., Mishra, P. Comparative study of some optimization techniques applied to Jacketed CSTR control. In *2015 4th International Conference on Reliability, Infocom Technologies and Optimization (ICRITO) (Trends and Future Directions)* 1–6 (IEEE, 2015). https://doi.org/10.1109/ICRITO.2015.7359368
15. Gupta, P., Kumar, V., Rana, K. P. S., Mishra, P. Velocity and position forms of self-tuning Fuzzy PI controller applied to jacketed CSTR. In *2015 Annual IEEE India Conference (INDICON)* 1–6. (IEEE, 2015). https://doi.org/10.1109/INDICON.2015.7443558
16. Maurya, P., Prasad, D. & Singh, R. S. Design of fractional-order sliding mode controller for an unstable three-state model jacketed CSTR. *Asia-Pac. J. Chem. Eng.* https://doi.org/10.1002/apj.3195 (2025).
17. Jana, A. K. Nonlinear state estimation and generic model control of a continuous stirred tank reactor. *Int. J. Chem. React. Eng.* https://doi.org/10.2202/1542-6580.1345 (2007).
18. Raja, G. L. Robust I-PD controller design with case studies on boiler steam drum and bioreactor. In *2023 15th International Conference on Computer and Automation Engineering (ICCAE)* 486–491 (IEEE, 2023). https://doi.org/10.1109/ICCAE56788.2023.10111205.
19. Mukherjee, D., Raja, G. L., Kundu, P. & Ghosh, A. Analysis of improved fractional backstepping and Lyapunov strategies for stabilization of inverted pendulum. *Sadhana* **49**, 48. https://doi.org/10.1007/s12046-023-02415-6 (2024).
20. Kumar, D. & Lloyds Raja, G. Generalized optimal 3-degree of freedom parallel cascade control strategy for stable, unstable and integrating chemical processes. *Chem. Eng. Sci.* **282**, 119243. https://doi.org/10.1016/j.ces.2023.119243 (2023).
21. Kumar, D. & Raja, G. L. Unified fractional indirect IMC-based hybrid dual-loop strategy for unstable and integrating type CSTRs. *Int. J. Chem. React. Eng.* **21**, 251–272. https://doi.org/10.1515/ijcre-2022-0120 (2023).
22. Kumari, S., Aryan, P., Kumar, D. & Raja, G. L. Hybrid dual-loop control method for dead-time second-order unstable inverse response plants with a case study on CSTR. *Int. J. Chem. React. Eng.* **21**, 11–21. https://doi.org/10.1515/ijcre-2022-0035 (2023).
23. Das, D., Chakraborty, S., Kumar, D. & Raja, G. L. Dual-loop PID control strategy for ramp tracking and ramp disturbance handling for unstable CSTRs. *Chem. Prod. Process Model.* **19**, 967–987. https://doi.org/10.1515/cppm-2024-0081 (2024).
24. Mukherjee, D., Raja, G. L., Kundu, P. & Ghosh, A. Improved fractional augmented control strategies for continuously stirred tank reactors. *Asian J. Control* **25**, 2165–2182. https://doi.org/10.1002/asjc.2887 (2023).

25. Aryan, P., Kumar, V., Raja, G. L., Chelliah, T. R. & Hote, Y. V. Robust shifted-IMC based modified decoupled Smith predictor for delay-dominant integrating-type chemical processes. *Int. J. Syst. Sci.* https://doi.org/10.1080/00207721.2025.2510313 (2025).
26. Mukherjee, D., Raja, G. L. & Kundu, P. Optimal fractional order IMC-based series cascade control strategy with dead-time compensator for unstable processes. *J. Control Autom. Electr. Syst.* **32**, 30–41. https://doi.org/10.1007/s40313-020-00644-2 (2021).
27. Mukherjee, D., Raja, G. L., Kundu, P. & Ghosh, A. Design of optimal fractional order Lyapunov based model reference adaptive control scheme for CSTR. *IFAC-PapersOnLine* **55**, 436–441. https://doi.org/10.1016/j.ifacol.2022.04.072 (2022).
28. Mukherjee, D., Raja, G. L., Kundu, P. & Ghosh, A. Fractional standalone backstepping control for nonlinear continuous stirred tank reactor. *Int. J. Robust Nonlinear Control* **35**, 7422–7437. https://doi.org/10.1002/rnc.70058 (2025).
29. Sharma, A., Kar, M. K. & Goud, H. A novel MGWO-based FOPID controller for CSTR system. *IETE J. Res.* **71**, 1396–1410. https://doi.org/10.1080/03772063.2025.2457356 (2025).
30. Siddiqui, O., Raja, G. L. & Chakraborty, S. Generalized IMC-PD decoupled dual-loop control of delay-dominated chemical systems using stability-constrained crayfish optimization. *J. Taiwan Inst. Chem. Eng.* **183**, 106563. https://doi.org/10.1016/j.jtice.2025.106563 (2026).
31. Chaturvedi, S., Kumar, N. & Kumar, R. A PSO-optimized novel PID neural network model for temperature control of jacketed CSTR: Design, simulation, and a comparative study. *Soft Comput.* **28**, 4759–4773. https://doi.org/10.1007/s00500-023-09138-0 (2024).
32. Deifalla, M. & Gasmelseed, G. Optimal temperature control for non-linear jacketed continuous stirred tank reactors using genetic algorithm. *J. Karary Univ. Eng. Sci.* https://doi.org/10.54388/jkues.v4i1.329 (2025).
33. Mjalli, F. S. & Jayakumar, N. S. An algorithm for stabilizing unstable steady states for jacketed nonisothermal continually stirred tank reactors. *Ind. Eng. Chem. Res.* **48**, 7631–7636. https://doi.org/10.1021/ie900072g (2009).
34. Rizk-Allah, R. M. et al. Enhanced PID controller tuning for nonlinear continuous stirred-tank heaters using a modified Newton-Raphson optimizer with random opposition and Lévy-flight learning. *Sci. Rep.* https://doi.org/10.1038/s41598-025-28802-z (2025).
35. Baldwin, D., Göktaş, Ü. & Hereman, W. Symbolic computation of hyperbolic tangent solutions for nonlinear differential–difference equations. *Comput. Phys. Commun.* **162**, 203–217. https://doi.org/10.1016/j.cpc.2004.07.002 (2004).
36. Fan, S.-K.S., Jen, C.-H. & Lee, T.-Y. Modeling and monitoring the nonlinear profile of heat treatment process data by using an approach based on a hyperbolic tangent function. *Qual. Eng.* **29**, 226–243. https://doi.org/10.1080/08982112.2016.1193614 (2017).
37. Zheng, F., Gong, H., Han, X., Hua, L. & Xin, S. Adaptive symmetry activation function for special Euclidean group: Theory and application. *Adv. Eng. Inform.* **70**, 104193. https://doi.org/10.1016/j.aei.2025.104193 (2026).
38. Hussein, N. K. et al. Schrödinger optimizer: A quantum duality-driven metaheuristic for stochastic optimization and engineering challenges. *Knowl. Based Syst.* **328**, 114273. https://doi.org/10.1016/j.knosys.2025.114273 (2025).
39. Izci, D., Jabari, M., Ekinci, S., Ghandour, R., Salman, M. Spider Wasp Optimizer-based PID control approach for temperature management in continuous stirred tank reactors. In *2025 9th International Symposium on Innovative Approaches in Smart Technologies (ISAS)* 1–5 (IEEE, 2025). https://doi.org/10.1109/ISAS66241.2025.11101837
40. Dochain, D. Process dynamics modeling, analysis, and simulation by B. Wayne Bequette 1st Edition, 1998; Prentice-Hall PTR, Upper Saddle River, New Jersey 07458, xviii + 621 pages; price $85,00 US. ISBN 0-13-206889-3. *Can. J. Chem. Eng.* **77**, 191–191. https://doi.org/10.1002/cjce.5450770131 (1999).
41. Henson, M. A. & Seborg, D. E. *Nonlinear Process Control* (Prentice Hall, 1997).
42. Xiao, F., Honma, Y. & Kono, T. A simple algebraic interface capturing scheme using hyperbolic tangent function. *Int. J. Numer. Methods Fluids* **48**, 1023–1040. https://doi.org/10.1002/fld.975 (2005).
43. Izci, D. et al. Dynamic load frequency control in power systems using a hybrid simulated annealing based quadratic interpolation optimizer. *Sci. Rep.* **14**, 26011. https://doi.org/10.1038/s41598-024-77247-3 (2024).
44. Akbari, E., Rahimnejad, A. & Gadsden, S. A. Holistic swarm optimization: A novel metaphor-less algorithm guided by whole population information for addressing exploration-exploitation dilemma. *Comput. Methods Appl. Mech. Eng.* **445**, 118208. https://doi.org/10.1016/j.cma.2025.118208 (2025).
45. Lang, Y. & Gao, Y. Dream optimization algorithm (DOA): A novel metaheuristic optimization algorithm inspired by human dreams and its applications to real-world engineering problems. *Comput. Methods Appl. Mech. Eng.* **436**, 117718. https://doi.org/10.1016/j.cma.2024.117718 (2025).
46. Al-Betar, M. A., Awadallah, M. A., Braik, M. S., Makhadmeh, S. & Doush, I. A. Elk herd optimizer: A novel nature-inspired metaheuristic algorithm. *Artif. Intell. Rev.* **57**, 48. https://doi.org/10.1007/s10462-023-10680-4 (2024).
47. Abdel-Basset, M., El-Shahat, D., Jameel, M. & Abouhawwash, M. Young's double-slit experiment optimizer : A novel metaheuristic optimization algorithm for global and constraint optimization problems. *Comput. Methods Appl. Mech. Eng.* **403**, 115652. https://doi.org/10.1016/j.cma.2022.115652 (2023).
48. Tulay, G., İskender, İ & Erdem, H. Optimal tuning of a boost PFC converter PI controller using heuristic optimization methods. *Int. Trans. Electr. Energy Syst.* **27**, e2458. https://doi.org/10.1002/etep.2458 (2017).
49. Ozgenc, B., Ayas, M. S. & Altas, I. H. Performance improvement of an AVR system by symbiotic organism search algorithm-based PID-F controller. *Neural Comput. Appl.* **34**, 7899–7908. https://doi.org/10.1007/s00521-022-06892-4 (2022).
50. Izci, D. & Ekinci, S. A novel-enhanced metaheuristic algorithm for FOPID-controlled and Bode's ideal transfer function-based buck converter system. *Trans. Inst. Meas. Control* **45**, 1854–1872. https://doi.org/10.1177/01423312221140671 (2023).

Author contributions

Davut Izci, Serdar Ekinci: Conceptualization, Methodology, Software, Visualization, Investigation, Writing-Original draft preparation, İrfan Ökten, Rıdvan Fırat Çınar, Mostafa Rashdan, Mohammad Salman, Burcu Bektaş Güneş and Mohd Ashraf Ahmad: Data cura-tion, Validation, Supervision, Resources, Writing - Review & Editing, Writing - Review & Editing.

Funding

This research received no external funding.

Declarations

Competing interests

The authors declare no competing interests.

Additional information

Correspondence and requests for materials should be addressed to M.S.

Reprints and permissions information is available at www.nature.com/reprints.